Apatite, monazite, and xenotime in metamorphic rocks

Frank S. Spear and Joseph M. Pyle

Department of Earth and Environmental Sciences

Rensselaer Polytechnic Institute

Troy, NY 12180 U.S.A.

INTRODUCTION

This chapter focuses on phosphates that are significant in metamorphic rocks. A quick survey of phosphate mineral descriptions at http://www.webmineral.com revealed over 500 phosphate mineral names. Remarkably, only three are common in metamorphic rocks: apatite, monazite, and xenotime, and this chapter is restricted to discussion of these minerals.

Apatite, monazite, and, to a lesser extent, xenotime, have enjoyed intensive study during the previous half-century. Following World War II, considerable study was made of minerals that contain fissionable materials, and the sometimes large concentrations of U and Th in monazite culminated in a number of seminal papers on the occurrence of that mineral (e. g. Overstreet, 1967). During the 1970s and early 1980s, the study of apatite and monazite turned towards their role as a sink for REEs

and other trace elements in rocks (e. g. Watson, 1980; Watson and Capobianco, 1981). Throughout this period, monazite (and to some extent xenotime) enjoyed attention as a geochronometer (e.g. Parrish, 1990), and through the 1990s, this attention has continued to grow.

Accessory minerals such as monazite, xenotime, and apatite have come to the forefront of research in metamorphic petrology in recent years for two reasons. First, it has recently been recognized that trace elements in metamorphic rocks, and especially trace element zoning in garnet and other major phases, contain considerable detailed information about the reaction history a rock has experienced. Coupled with the fact that diffusion of many trace elements in metamorphic minerals is, in general, considerably slower than diffusion of major elements in those same minerals, the possibility has recently emerged of recovering details of metamorphic petrogenesis that were previously unattainable. Inasmuch as accessory minerals play a dominant role in mass budget of many trace elements, attention has naturally turned to their paragenesis. It has also recently been discovered that accessory minerals themselves contain a paragenetic record in their chemical zoning profiles, adding further impetus to their study.

Second, the past decade has seen the development of *in situ* dating techniques (e. g. SIMS, LA-ICP-MS, and EMP) that make it possible to obtain Th/Pb, U/Pb, or Pb/Pb ages on individual spots in a grain of monazite or zircon. This is significant for two reasons. Firstly, *in situ* dating permits correlation of the age of a mineral and its textural setting. For example, it is possible to measure the age difference between monazites that are included within garnet and those in a rock's matrix (e.g. Catlos et al., 2001;

Foster et al., 2000). Secondly, the complex chemical zoning observed in monazite and zircon require a technique that permits age determination on individual chemical zones within a crystal, otherwise mixed ages are inevitable.

Research is currently focused on the melding of these two approaches. A major goal of accessory mineral studies in metamorphic rocks is the determination of age, P, and T on an individual spot in a mineral such as monazite. In principle, this should be possible. Monazite records chemical evidence of involvement in major-phase reactions, for which P and T information may be gleaned by conventional methods. Monazite itself contains temperature-sensitive information in its Y and HREE content if it coexists with xenotime (i.e. the monazite-xenotime miscibility gap; Heinrich et al., 1997; Seydoux-Guillaume et al., 2002) or garnet (garnet-monazite net transfer thermometry; Pyle et al., 2001). Measurement of an age in a monazite growth zone for which P and T have been determined results in a specific P-T-t point in a rock's history. Two or more such points results in such fundamental information as heating and burial rates and would provide quantitative constraints on the rates of tectonic processes.

This chapter was written to provide a summary of the current state of knowledge on metamorphic monazite, xenotime, and apatite. Details of geochronological approaches are addressed elsewhere (Harrison et al., this volume), and this chapter will focus on petrology. The chemistries of these minerals will be summarized, and examples of zoning and paragenesis presented. As will be seen, much is as yet unknown about the behavior of these accessories during metamorphism, and directions for future research to address the outstanding questions will be discussed.

OCCURRENCE AND CHEMISTRY OF METAMORPHIC APATITE, MONAZITE AND XENOTIME

Electron microprobe analysis of apatite, monazite, and xenotime

The first issue with respect to analyzing accessory phosphates is to obtain accurate chemical analyses. This is not a simple task. Rare-earth and other elements in these phosphates have a large number of X-ray peaks with numerous overlaps, and accurate analysis using the electron microprobe (EMP) takes considerable care in selecting X-ray lines and locating background measurements. Apatite is additionally problematic because of the rapid diffusion of F under the electron beam (e.g. Stormer et al., 1993), a problem that affects accurate analysis of all elements. These issues must be kept in mind when evaluating published analyses of metamorphic phosphates. Details of analytical methods for the analysis of metamorphic phosphates using the EMP are discussed elsewhere in this volume (Pyle, et al., this volume).

Apatite

Although apatite has been intensely studied for such diverse applications as fission track dating and igneous petrogenesis (this volume), studies concerned exclusively with compositional variation of metamorphic apatite are relatively few in number in comparison to the other types of apatite-focused studies in the literature (e.g. Kapustin, 1984). Apatite papers applicable to metamorphic rocks include studies of the fugacity of components in metamorphic fluids in apatite-bearing samples (Korzhinskiy, 1981; Yardley, 1985; Smith and Yardley, 1999), apatite-biotite OH-F exchange thermometry (Stormer and Carmichael, 1971; Ludington, 1978; Sallet and Sabatier, 1996; Sallet, 2000), and apatite-fluid partitioning (Zhu and Sverjensky, 1991, 1992; Brennan, 1993).

Studies of metamorphic apatite composition generally focus on either halogen content (e.g., Yardley, 1985; Smith and Yardley, 1999) or REE content (e.g. Cruft, 1966; Puchelt and Emmerman, 1976; Bingen et al., 1996), although some studies present a more or less complete apatite analysis including Ca, P, halogens, and REEs (e.g. Bea and Montero, 1999).

The literature data presented in this chapter represent a wide variety of metamorphic rock types including metabasites, metapelites, marbles, calc-silicate rocks, ultramafic rocks, and metagranites. Hydrothermal or low-temperature apatite occurrences were not considered for this chapter.

Occurrence and stability. Apatite $Ca_5(PO_4)_3(OH,F,Cl)$ is common in rocks of diverse bulk composition, having been reported in metamorphic rocks of pelitic, carbonate, basaltic, and ultramafic composition. The essential constituents of apatite are present in amounts greater than trace quantities in these types of rocks, and apatite forms easily as a result.

Apatite is found at all metamorphic grades from transitional diagenetic environments and low-temperature alteration to migmatites, and in ultra high-pressure (diamond-bearing; e.g., Liou et al., 1998) samples. A list of all papers that report metamorphic apatite would be prohibitively long. The occurrence of apatite is not apparently dictated by its stability relative to other phosphates, but, rather by the availability of essential constituents (P, Ca, and F).

Apatite composition. The compositions of metamorphic apatite typically fall along the F-OH join, although apatite with small amounts of Cl has been reported from metamorphic rocks (e.g. Kapustin, 1987). Most, if not all, metamorphic apatite is

dominated by the F end-member (i.e. fluor-apatite). A survey of analyses is shown in Figs. 1 and 2. The F/(F+OH) typically ranges from 0.4 to 1.0 with a median value of 0.85 (Fig. 1a). Thus, it appears that the widespread presence of apatite in metamorphic rocks may be as much a function of the availability of F as it is the availability of P. (It should be noted that many published apatite analyses have reported F values in excess of the maximum permitted by stoichiometry, presumably due to analytical difficulties measuring F in apatite on the EMP as discussed by Stormer et al., 1993).

Figure 1b shows the compositions of metamorphic apatite separated by metamorphic grade from Kapustin (1987). The analyses were obtained by wet chemistry, circumventing the problems with F analysis that are exhibited by microprobe analyses. As can be seen from the plots, the composition of metamorphic apatite appears to be a function of grade. The greenschist facies apatites have modest Cl contents and F/(F+OH) of 0.80-0.94. By the granulite facies, apatites are virtually Cl-free, and the F/(F+OH) is 0.94-0.98. The strong preference of metamorphic apatite for F over Cl can be understood in the context of F-Cl-OH partitioning between apatite and fluid (see below), and the decrease in Cl with grade could be due to Rayleigh distillation of Cl accompanying dewatering of the metamorphic rocks.

The minor elements Fe, Mg and Mn are in concentrations less than 0.1 cations/8 oxygens (Fig. 2a-d). Additionally, there appears to be a systematic relationship between Fe/(Fe+Mg) of apatite and coexisting phases, which has potential for petrogenetic studies. Y and LREE concentrations are also typically low (Fig. 2e, 2f), but sometimes show zoning (see below). Apatite coexisting with monazite in pelitic samples typically contains much lower concentrations of REEs (Pyle, 2001; Yang and Rivers, 2002) than

does apatite in marbles and metaperidotites (Cruft, 1966) or metabasalts (Bingen et al., 1996) with or without allanite. However, spuriously high REE concentrations in apatite may arise from analysis of minute inclusions of REE-rich phases (monazite, xenotime) (Amli, 1975; Bea et al., 1994). Therefore, apatite REE compositional data derived from non *in situ* analytical methods are suspect (Cruft, 1966), and even *in situ* derived analytical data must be viewed with caution (Bea et al., 1994). REE patterns of metamorphic apatites (Fig. 3a, d) are relatively flat or display minor HREE depletion.

Compositional zoning. Zoning has been described in some metamorphic apatite crystals (Fig. 4), although most crystals examined by the authors display little or no zoning in BSE images taken at up to 100 nA current (unpublished results). Smith and Yardley (1999) report zoned apatites that were interpreted as having detrital cores (Fig. 4a). Yang and Rivers (2002) report Y zoned apatite crystals with cores higher than rims (Fig. 4b). Apatite from a leucosome in a migmatite from central New Hampshire (Figs. 4c, 4d; unpublished data of the authors') displays zoning in F and Fe/(Fe+Mg). No zoning of P, Y, or Ca was observed in this crystal. The Fe/(Fe+Mg) zoning is believed to reflect growth zoning during melt crystallization.

Monazite and xenotime

Occurrence and stability. Monazite, (LREE)PO_4, and xenotime (Y,HREE)PO_4 are common in metapelitic rocks and less abundant in mafic and calcic bulk compositions. Monazite and xenotime occur as detrital grains (beach sands comprised largely of monazite are reported) but are apparently not stable during diagenesis (e.g. Overstreet, 1967), except as detrital grains (Suzuki and Adachi, 1991; Suzuki et al., 1994; Hawkins and Bowring, 1999; Catlos et al., 2001; Rubatto et al., 2001; Ferry, 2000; Wing et al.,

2002). Monazite appears to be stable in rocks of appropriate bulk composition at all metamorphic grades at and above the greenschist facies. Monazite has been reported from low-pressure contact aureoles (e.g. Ferry, 2000; Wing et al., 2002), cordierite + K-feldspar rocks (e.g. Franz et al., 1996), granulite facies migmatites (e.g. Watt and Harley, 1993; Bea et al., 1994; Hawkins and Bowring, 1999; Pyle et al., 2001), and pelitic rocks of ultra high-pressure (diamond-bearing) metamorphic facies. For example, Terry et al. (2000) report monazite in coesite-bearing eclogites from western Norway. Furthermore, Liou et al. (1998) report monazite exsolution from apatite from a sample of ultra high-pressure clinopyroxenite from the Dabie Shan, China, which suggests that the solubility of REEs in apatite (i.e. monazite components) increases with increasing pressure.

Xenotime is reported from rocks of the chlorite zone to the cordierite + K-feldspar zone (e.g. Franz et al., 1996). Pyle and Spear (1999) report on xenotime textural occurrences in a suite of metapelitic samples from central New England that range in grade from garnet through cordierite + garnet zone. In the garnet zone, xenotime is common in the matrix of the rock and as inclusions within garnet. In garnet-bearing rocks, xenotime reacts out as garnet grows and is often consumed by the mid-garnet zone (Fig. 5a). Because of the incorporation of Y and HREEs into garnet, xenotime is often not present in the matrix of garnet-rich rocks above the mid garnet zone, although it may still be present as inclusions within garnet. Matrix xenotime appears again in some rocks of the migmatite zone as a product of melt crystallization (Fig. 5d). Finally, alteration of Y-rich garnet may release sufficient Y to stabilize xenotime during

retrogression (Fig. 5b, c). In garnet-absent samples, xenotime may persist throughout all metamorphic grades (e. g. Bea and Montero, 1999; Pyle and Spear, 1999).

The crystal size of monazite and xenotime tends to increase with increasing metamorphic grade (e.g. Franz et al., 1996; Rubatto et al., 2001). Ferry (2000) and Wing et al. (2002) report xenoblastic monazite at lower grades in a contact aureole, a low-P Buchan terrane, and a Barrovian terrane, which is replaced by allanite with increasing grade before an idioblastic variety appears at the Al_2SiO_5 isograd.

A detailed discussion of the paragenesis of monazite and xenotime in metamorphic rocks will be taken up below.

Composition. Monazite has the nominal composition (LREE)PO_4 and the LREEs (primarily La + Ce + Nd) generally comprise approximately 75% of the total cation proportions (exclusive of P) of most metamorphic monazites (Fig. 6). Indeed, the range of observed LREE concentrations is quite restricted (Figs. 6, 8a, 10a) with La, Ce and Nd averaging around 0.2, 0.43, and 0.17 cations/4 oxygens, respectively. Most monazites also contain additional Th, U, Ca, Si, HREEs, Y, and Pb. Y concentrations up to 0.1 cations/4 oxygens have been reported (e.g. Heinrich et al., 1997), although HREE concentrations are generally less than 0.02 cations/4 oxygens (Fig. 6e, 10a,b).

Xenotime has the nominal composition YPO_4, and Y comprises 75-85% of the total (Fig. 7a) with the HREEs comprising the bulk of the remainder (Fig. 7b-e; Fig. 8b, c; Fig 10c, d). The range of HREE contents is actually rather restricted with Gd, Dy, Er, and Yb all showing a limited range of concentrations (Figs. 7, 8, 10c,d). As discussed below, Y and HREE concentrations in monazite coexisting with xenotime are temperature sensitive and may be used for geothermometry.

REE patterns of metamorphic monazite (Fig. 3b, e) have negative slopes, sometimes with a negative Eu anomaly. Xenotime shows a "dog leg" pattern with a positive slope through the MREEs and flat in the HREEs (Fig. 3c, f).

Th and U are found in metamorphic monazites with concentrations that range up to 0.25 atoms per four oxygen formula unit, although most metamorphic monazites have less than 0.05 atoms (Fig. 9a, 10b). U concentrations range up to approximately 0.01 atoms per formula unit, but most are less than 0.005 atoms (Fig. 9b). Xenotime Th and U concentrations are much more restricted with the maximum being approximately 0.02 and 0.01 atoms per formula unit, respectively (Fig. 9c,d; 10d).

Pb is present in metamorphic monazite and xenotime, but it is believed that nearly all of the Pb is radiogenic (e.g. Parrish, 1990). The amount of Pb depends on the initial concentrations of Th and U and the age of the sample, and values greater than 1 wt% have been measured (see Harrison et al., this volume).

Exchange vectors in monazite and xenotime. Y substitutes for REEs with the uncoupled substitution

Y = REE

Th and U both have charges of +4 compared with the +3 charge of the REEs and require coupling to achieve charge balance. Two substitutions that have been proposed are

Th or U + Si = REE + P (huttonite in monazite; thorite in xenotime)

with Si replacing P in the tetrahedral site and

Th or U + Ca = 2REE (brabantite)

with Ca replacing an additional REE in the 8-fold site.

Figure 11 shows plots of Th + U, Ca, and Si for monazite to illustrate the exchange vectors. Figure 11a shows an excellent correlation between Th + U versus Si + Ca, indicating that nearly all of the Th + U can be accommodated by the two substitution mechanisms. Figures 11b and c show that the brabantite substitution dominates in monazite. This can be seen even more clearly in Figures 11d and 11e. Figure 11d shows the residual Th + U after the huttonite component is subtracted, and the strong correlation with Ca is evident. In Fig. 11e the contribution of the brabantite component has been subtracted from Th + U and it can be seen that there is very little residual Th + U that needs to be accommodated. A trend in a subset of the data, however, indicates that in some samples the huttonite substitution may be important.

Plots of xenotime compositions show much less obvious correlations (Fig. 12). Figure 12a reveals that there is an excess of Si + Ca over what is required for incorporation of Th + U. The plot of Ca against Th + U (Fig. 12b) reveals no obvious correlation, but the plot of Si against Th + U reveals an excess of Si over what is required for charge balance. This suggests that Si is incorporated into metamorphic xenotime by an additional substitution mechanism suspected to be the zircon substitution:

$Zr + Si = REE + P$ (zircon).

Zircon and xenotime have the same structure, and solid solution between these phases is evident (e.g., Görz and White, 1970; Romans et al., 1975; Bea, 1996). Unfortunately, there are no complete analyses of metamorphic xenotime that include Zr, so this suggestion must remain speculative.

Chemical zoning in monazite. A large number of papers have reported chemical zoning in metamorphic monazite (e.g. Watt and Harley, 1993; Crowley and Ghent, 1999; Williams et al., 1999; Zhu and O'Nions, 1999a; Hawkins and Bowring, 1999; Bea and Montero, 1999; Ayers et al., 1999; Townsend et al., 2000; Pyle et al., 2001). Zoning in monazite is often readily apparent in back-scatter electron (BSE) images. Based on a survey of monazites from two samples of high grade gneisses from the Lewisian terrain, Scotland, Zhu and O'Nions (1999a) identified three distinct zoning types in monazite: concentric, patchy, and "intergrowth-like". Representative examples of each are shown in Figure 13a-e. Concentric zoning was the most common and was observed to be either simple (Fig. 13a) or complex (Figs. 13b, c). Rims were typically higher in Th but the opposite (low-Th rims) was also observed. Line traverses (Fig. 13f, g) across two grains showing concentric zoning (Fig. 13b, c) reveal distinct chemical domains with sharp boundaries. Furthermore, Th and U concentrations are positively correlated with Ca and Si and are negatively correlated with the LREEs (La, Ce, Sm, Nd), supporting the brabantite and huttonite substitution mechanisms discussed above. Pb is also positively correlated with Th and U. Most important are the sharp boundaries between the chemical domains, which suggests that post-crystallization diffusional modification of the zoning is below the spatial resolution of the electron microprobe (approximately 2 μm).

The correlation of Th and U with Si is shown dramatically in the X-ray maps of Figure 14. An intermediate zone in this monazite crystal has a euhedral outline with initially high Th, which decreases steadily outward. Si zoning (Fig. 14b) matches the

Th zoning perfectly. U is only weakly zoned, but shows a similar pattern. Y zoning is indistinct, and does not show the sharp chemical zones seen in Th and Si.

Zoning in monazite from schists ranging from garnet to migmatite grade from west-central New Hampshire, USA, is shown in Figure 15 (Pyle, 2000; Pyle et al., 2001). Typical garnet zone monazite has a high-Th core with little zoning of Y (Fig. 15a, b, c). Sillimanite zone monazites often show low-Th, high-Y overgrowths (Figs. 15d, e, f). The most complex zoning was observed in monazite from the migmatite zone (Figs. 15g-l). These high grade monazites are characterized by a number of distinct growth zones, which can be seen as chemically distinct zones, especially on Y maps (Figs. 15h, 15k). In one suite of samples from cordierite + garnet migmatites from central New Hampshire, as many as four distinct growth zones in a single monazite grain have been documented (Fig 15k). These high-grade monazites are interpreted to have undergone a series of growth and resorption reactions throughout their history, which can be correlated with reactions involving major phases in the rock. Similarly complex zoning in high-grade monazite was reported by Bea and Montero (1999) and Hawkins and Bowring (1999).

Compositionally distinct material observed in the cores of some migmatite zone monazite crystals (e.g. Figs. 15g,h,i) could readily be interpreted as representing the initially-formed monazite core. However, Pyle et al. (2001) have suggested that this texture, in some instances, may arise from an extremely irregular crystal shape and the orientation of the thin section cut through the crystal (Fig. 16). Monazite at low grades is often embayed due to either irregularities in growth in different directions, or to resorption due to monazite-consuming reactions. A highly embayed monazite crystal

(Fig. 16a) that experiences later growth that fills in the embayments, would, after cutting in certain orientations, have the appearance of an internal core with a composition similar to the rim. Thus, what appears at first to be four distinct growth zones is, in fact, only two with a complex geometry of the core region. Interpretations of the growth history of monazite in complexly zoned grains must take into consideration this possibility.

Several generalizations can be made based on zoning observed in BSE and X-ray images of monazite:

1. Th and U zoning are correlated with Ca, Si, and LREE zoning, consistent with the proposed exchange mechanisms;
2. Th and U are often zoned, but their zoning is not always correlated;
3. Pb is correlated with Th and U concentrations;
4. Y zoning is sometimes similar to Th (and U) zoning, but is sometimes uncorrelated. Y zoning is believed to record a history of monazite growth in many cases.
5. Zoning observed in BSE images is sometimes due to zoning in Th and/or U and sometimes due to zoning in Y. Grains must be tested individually by spot analyses or X-ray mapping to determine the cause of BSE zoning.
6. Very sharp boundaries exist between chemically distinct zones. This is especially true of Th, U, Si, Ca and Pb zoning. Y zoning is also typically sharp, but sometimes not as distinct as the others. That is, there is no evidence for diffusional homogenization, despite the high metamorphic grade of some samples.

This last observation has important implications with respect to monazite geochronology (e.g. Harrison et al., this volume). The available evidence from natural

monazites, including those from the granulite facies, suggests that diffusion has not modified the chemical zoning, including that of Pb. The implication of this observation is that the closure temperature of monazite for Th-U-Pb geochronology is above 800 ˚C, consistent with the recent diffusion study of Cherniak et al. (2000).

Chemical zoning in xenotime. Chemical zoning in xenotime is not easy to observe because most metamorphic crystals are smaller than 20 μm. An exception is a 300 μm xenotime described by Viskupic and Hodges (2001), which is zoned in BSE imaging (Fig. 17a). Although no X-ray maps are available for this xenotime, spot analyses reveal that the BSE contrast is due to variations in Y (and presumably HREEs) content. Figures 17b and 17c are BSE images of two xenotimes in kyanite-bearing metaquartzite from New Mexico (C. Daniel and J. Pyle, unpublished data). X-ray maps of one of these (Fig. 17b) reveal chemical zoning similar to the observed BSE contrast (Fig. 18). Zoning in P, Y, Yb and Dy mimic the BSE contrast. The HREEs Yb and Dy are antithetic to Y, and the zoning in P reflects the change in average atomic weight of the crystal due to the substitution of HREEs for Y. That is, there is no evidence that this crystal has less than 1.0 P/formula unit, but the weight per cent of P must change to accommodate the other substitutions. Si and U are zoned sympathetically, but do not correlate as a whole with variation in the other elements. The correlation of Si and U supports the substitution mechanism Si + U = P + REE. Additionally, the elements Th, Zr, Ca, and Yb were mapped but show no visible variation.

Age zoning in monazite. Numerous studies have reported age zoning in monazite, based on SIMS analysis, TIMS analysis on parts of individual monazite grains, and X-ray mapping of Th, U, and Pb, coupled with EMP spot age determinations (e.g. Parrish,

1990; Williams et al., 1999; Crowley and Ghent, 1999; Terry et al., 2000). Geochronology of phosphate minerals is addressed in detail elsewhere in this volume, but examples that show the texture of the age zoning based on EMP analysis and X-ray mapping are discussed here to illustrate the relationship between compositional zoning and age zoning in monazite (e.g. Williams et al., 1999).

Figure 19 illustrates two examples of age zoning in monazite. The grain illustrated in Figures 19a-c is from a sample of ultra high-pressure gneiss from the Western Gneiss Region, Norway (Williams et al., 1999; Terry et al., 2000). The core of the grain displays irregular, patchy zoning in Th and U with three distinct concentrations of Th separated by sharp boundaries. The rim is a fourth chemical zone. The age map shows two distinct age zones, the core at approximately 1.05 Ga and the rim at 400 Ma (Fig. 19c, d). Particularly revealing is the observation that, despite the complex Th zoning in the core of the monazite, the calculated ages are all relatively similar (i.e. 1.05 Ga). That is, the zoning present in the core must have originated during a Grenville metamorphic event and survived ultra high-pressure metamorphism during the Caledonian.

The second example (Fig. 19 e and f), from Crowley and Ghent (1999), shows a monazite from the Monashee complex, southern Canadian Cordillera, with a low Th and Pb core surrounded by a high Th rim. The Pb concentration is low in the core, increases in the near-rim and plummets at the rim. The age plot (Fig. 19f) reveals a relatively constant age of 1935 Ma from the core to the rim with the age plummeting to around 50 Ma at the rim. This age zoning is impossible to predict by examination of the

BSE image (Fig. 19e), and it is worth noting that there is no evidence in these samples for modification of the ages due to diffusion of Th, U, or Pb.

CRITERIA FOR EQUILIBRIUM BETWEEN COEXISTING PHOSPHATES AND OTHER PHASES

There are special considerations that must be borne in mind when interpreting the compositions and zoning in metamorphic phosphates and certain other minerals. Petrologists are familiar with the concept of a refractory phase in rocks undergoing melting: refractory phases do not melt and are left in the residue or "restite". In solid state reactions, "refractory" implies a reluctance to react, which carries a kinetic connotation. For the purposes of this discussion, we wish to present another definition that focuses on the ability of a solid solution phase to maintain a homogeneous composition during reaction. Most reactions involving solution phases result in changes in composition of those phases as the reaction proceeds. Solution phases that possess rapid diffusivity can change their internal composition through intragranular diffusion so that the interior of the phase has the same composition as the reacting rim. Solution phases with slow diffusivities do not homogenize as reaction proceeds, leading to zoned crystals if the phase is a product in the reaction. Garnet is an excellent example of this phenomenon in a metamorphic rock.

Accessory phosphates possess relatively low diffusivities for many elements under metamorphic conditions, based on the presence of nearly ubiquitous chemical zoning (Suzuki et al., 1994) and corroborated by experimental determinations of trace element (REEs, U, Pb, Th) diffusivities in phosphates (e.g. Smith and Giletti, 1997; Cherniak,

2001). Chemical zoning has been reported in apatite (Fig. 4), monazite (Fig. 13-16), and xenotime (Figs. 17 and 18), and unzoned crystals are the exception rather than the rule. Special considerations apply when evaluating equilibrium between two phases with slow internal diffusivities. If both phases are growing during reaction, then the outer shell of both phases can be considered to be in equilibrium. However, if one phase is growing at the expense of the other, then it is likely that no measurable part of either phase is in equilibrium with the other. Even if intragranular transport is rapid such that local equilibrium between the outer, infinitesimal rim of each phase is in equilibrium, the interiors of the phases will not be. Considering that the electron microprobe is only capable of measuring to within approximately 1-2 μm of the rim of a mineral, the equilibrated parts may not be measurable.

Figure 20 shows four possibilities for reaction between two phases with slow diffusivities. Of the four possible reaction histories shown in the figure, the only combination that yields coexisting equilibrium compositions is the one in which both phases grow (Fig. 20a).

The point of this discussion is to emphasize that the mere presence of a mineral such as monazite, xenotime or apatite does not ensure that it is part of an equilibrium assemblage. For example, the presence of an included phase such as monazite inside of a garnet porphyroblast does not assure two-phase equilibrium between these phases. Furthermore, the complexity of zoning observed in monazite, xenotime and apatite suggest complex reaction histories with several episodes of growth and resorption. It is not a simple task to relate a specific growth zone within one phase (e.g. monazite) to having formed in equilibrium with any other phase. This point is especially significant

when one attempts to apply monazite-xenotime, xenotime-garnet, or monazite-garnet thermometry, which requires equilibration between the phases to be valid. Indeed, achieving the goal of obtaining an age and a metamorphic temperature from a single spot on a monazite (e. g. Viskupic and Hodges, 2001) requires careful evaluation of equilibrium.

Several approaches may be utilized to assess equilibrium including textural analysis, examination of element partitioning, evaluation of chemical zoning, and thermodynamic modeling. Pyle et al. (2001) addressed the issue of textural equilibrium between monazite and xenotime and between monazite and garnet and proposed the criteria listed in Tables 1 and 2, ranked in order of confidence level. Because of the limited diffusivities in these three minerals, however, textural criteria alone are not particularly robust indicators of chemical equilibrium, and need to be combined with other approaches, as discussed below.

ELEMENT PARTITIONING BETWEEN COEXISTING PHOSPHATES AND OTHER PHASES

The study of partitioning of elements between and among metamorphic phases has two useful objectives. First, it is a means of ascertaining whether the compositions are consistent with the phases having achieved chemical equilibrium. Second, the partitioning may be sensitive to temperature and/or pressure, and thus be useful for thermobarometry.

Several studies have reported on the partitioning of various elements between coexisting metamorphic phosphates and between phosphates and other metamorphic phases, and are summarized here.

Monazite - xenotime partitioning

Franz et al. (1996) present a plot of element distributions between monazite and xenotime formulated as $K_D = (El_{Mnz}/El_{Xno})$, which is reproduced here with modification in Figure 21. Monazite strongly favors the LREEs with $\log(K_D)$ values between 2.5 and 3.5, whereas xenotime favors the HREEs with $\log(K_D)$ between -0.5 and –2.5. Si is favored slightly in monazite, which also strongly partitions Th with $\log(K_D)$ between 1 and 2. U partitioning is variable. In some samples, U is favored in monazite, whereas in others it is favored in xenotime.

Figure 22 shows compositions of coexisting monazite and xenotime from a suite of metapelitic rocks from central New England (Pyle and Spear, 1999; Pyle et al., 2001). Criteria used to select pairs of coexisting phosphates are those listed in Table 1. In general, there is a regular array of tie lines between monazite and xenotime, and monazite with the highest HREE concentrations coexist with xenotime with the highest HREE concentrations. The range of Y concentrations displayed by monazite coexisting with xenotime is a function of metamorphic grade, as will be discussed below.

Partitioning of Y, Gd, and Dy between monazite and xenotime as a function of metamorphic grade has been discussed by Pyle et al. (2001) (Figure 23). In this study, K_{eq} is defined as the equilibrium constant for the two exchange reactions

$(Gd, Dy)PO_4(Mnz) + YPO_4(Xno) = YPO_4(Mnz) + (Gd,Dy)PO_4(Xno)$

as

$$K_{eq} = \frac{\left(\frac{X_{YPO_4}}{X_{(Gd,Dy)PO_4}} \right)_{Mnz}}{\left(\frac{X_{YPO_4}}{X_{(Gd,Dy)PO_4}} \right)_{Xno}}.$$

The variation in K_{eq} across metamorphic grade (Fig. 23) is small. Although there is a small increase in Keq with grade for the Y-Dy equilibrium constant, the variation is within analytical uncertainty.

Monazite-xenotime miscibility gap. A number of studies have documented the temperature dependence of Y or Y + HREEs in monazite coexisting with xenotime, and suggested its application as a geothermometer (Gratz and Heinrich, 1997, 1998; Andrehs and Heinrich, 1998; Heinrich et al., 1997; Pyle et al., 2001; Seydoux-Guillaume et al., 2002). An accurate thermometer based on monazite composition would be an enormously valuable tool because it would open the possibility of obtaining a temperature-time point on a single mineral grain, with obvious application to petrogenesis, thermochronology, and tectonics.

Figure 24 reproduces the experimental and empirical data on the monazite-xenotime miscibility gap. The diagrams have been redrafted from the originals to the same scale to facilitate comparisons. Gratz and Heinrich (1997; Fig. 24a) reported on an experimental study in the simple $CePO_4$-YPO_4 system. The miscibility gap is modestly pressure sensitive and displays a temperature sensitivity that permits temperature estimates to approximately ±25 ˚C, provided the effects of additional components are properly accounted for. Heinrich et al. (1997; Fig. 24b, solid symbols)

and Pyle et al. (2001; Fig. 24c) report empirical miscibility gaps where the temperatures were estimated from phase relations and thermometry in the samples. Both studies show gaps with similar trends, but the Pyle et al. (2001) data show slightly higher Y + HREEs at a given temperature than do the data of Heinrich et al. (1997). Andrehs and Heinrich (1998) conducted experiments in which the partitioning of Y + HREEs was measured between monazite and xenotime of more or less natural compositions (Fig. 24b, open symbols). These data show a narrower gap than do the natural data at temperatures below 600 ˚C, the cause of which, although unknown, is likely to be the presence of additional components such as Ca, U, Si, and Th in the natural monazites. Seydoux-Guillaume et al. (2002; Fig. 24d) examined experimentally the effect of the $ThSiO_4$ substitution on the monazite-xenotime gap. Incorporation of Th into monazite narrows the gap somewhat, and is clearly an important consideration in the application of monazite-xenotime thermometry. Seydoux-Guillaume et al. (2002) also present phase diagrams for the system $CePO_4$ – YPO_4 – $ThSiO_4$ (Fig. 25) in which they illustrate the effect of the $ThSiO_4$ component in the ternary system and show the limit of $ThSiO_4$ substitution at thorite saturation.

Accuracy of the monazite-xenotime thermometer is difficult to assess at this time. It is clear that HREEs and $ThSiO_4$ affect the position of the gap relative to the pure $CePO_4$-YPO_4 system. The brabantite component ($CaTh(PO_4)_2$), which is responsible for significant Th and U substitution into monazite, may also be significant, but its effect has not been examined. A solution model for monazite that incorporates the major compositional effects is an obvious goal for future research. Equally important, it must be emphasized that unless it can be documented that xenotime was, in fact, in

equilibrium with monazite (not always easy to do), the thermometer can only give minimum temperature estimates. Nevertheless, the potential of this thermometer is large, and merits considerable further study.

Xenotime/monazite – garnet Y distribution

Yttrium partitions strongly into garnet relative to other silicates. Pyle and Spear (2000) report a strong correlation between metamorphic grade and the Y concentration in garnet coexisting with xenotime (Fig. 26a), and Pyle et al. (2001) describe a similar relationship for garnet coexisting with monazite (Fig. 27). Two semi-empirical thermometers were derived (Figs. 26b and 27) that are based on compositions measured in a well-characterized suite of samples from central New England.

A net transfer reaction can be written among garnet, apatite, quartz, plagioclase and fluid that describes the dependence of Y concentration in garnet on grade:

$$\underset{\text{YAG (in Grt)}}{Y_3Al_2Al_3O_{12}} + \underset{\text{OH-Apatite}}{Ca_5(PO_4)_3(OH)} + 25/4\ \underset{\text{Qtz}}{SiO_2} =$$

$$3\underset{\text{Xno or Mnz}}{YPO_4} + 5/4\underset{\text{grs (in Grt)}}{Ca_3Al_2Si_3O_{12}} + 5/4\underset{\text{an (in Pl)}}{CaAl_2Si_2O_8} + 1/2\underset{\text{fluid}}{H_2O}$$

The YAG-xenotime thermometer is based solely on the Y concentration (in ppm) in garnet (Fig. 26b), but the YAG-monazite thermometer incorporates activity models for the components of the above reaction (Fig. 27). The systematics of the YAG-xenotime thermometer imply that the activities of YPO_4 in xenotime, OH-apatite, and H_2O are relatively constant and that the activity product of grossular and anorthite is relatively constant. For the YAG-monazite thermometer, measured compositions of YPO_4 in monazite, grossular in garnet, anorthite in plagioclase, and OH in apatite (via

subtraction of F- and Cl- components) were used, but a constant activity of H_2O was assumed.

These thermometers are quite sensitive to changes in temperature. In the garnet zone, the YAG-xenotime thermometer has a sensitivity of only a few degrees, based on analytical precision of ±100 ppm (Fig. 26c). At higher grades, the temperature sensitivity is considerably worse, increasing to several tens of degrees by the sillimanite zone conditions, owing to the much smaller Y concentrations of garnet at higher grades (Fig. 26c). The YAG-monazite thermometer has larger uncertainty (±20-30 degrees in the garnet zone) because of the smaller concentration of YPO_4 in monazite as compared with xenotime and the similarly smaller concentrations of YAG in garnet. More sensitive analytical methods to measure YAG in garnet such as LA-ICP-MS would reduce these errors, especially in higher grade samples where the YAG concentrations in garnet are lowest.

Apatite-fluid and apatite-biotite partitioning

F and Cl are partitioned between apatite, metamorphic fluids, and micas, and a number of studies have examined this partitioning as either a monitor of fluid composition (e.g. Yardley, 1985; Sisson, 1987; Nijland et al., 1993; Smith and Yardley, 1999) or as a geothermometer (e.g. Stormer and Carmichael, 1971; Luddington, 1978; Zhu and Sverjensky, 1992; Sallet, 2000).

F is partitioned into apatite considerably more strongly than is Cl (Fig. 28). Smith and Yardley (1999) calculated a species predominance diagram based on data in Zhu and Sverjensky (1992) that illustrates the magnitude of this partitioning. For example, at the intersection of the three equal molar lines in Figure 28a, the composition of the

apatite is $X_F = X_{Cl} = X_{OH} = 1/3$ (assuming ideal mixing). The fluid composition at this point has activity ratios of $a_{HF}/a_{H2O} = 10^{-5.2}$ and $a_{Cl}/a_{H_2O} = 10^{-2.8}$. That is, the fluid has over two orders of magnitude more Cl than F, despite their equal concentrations in apatite. This can also be seen in the isopleth diagrams calculated assuming ideal mixing (Figs. 28b, c, d). F-rich apatites (e.g. with F-apatite compositions greater than 0.9 X_F) are in equilibrium with relatively dilute metamorphic fluids ($a_{HF}/a_{H_2O} < 10^{-4}$) (Fig. 28b), whereas fluids with $a_{HCl}/a_{H_2O} < 10^{-4}$ are in equilibrium with apatite with $X_{Cl} <$ 0.1 (Fig. 28c). This strong partitioning accounts for the observation that metamorphic apatite is typically F-rich (i.e. Fig. 1; Smith and Yardley, 1999), in contrast to igneous apatites, which are commonly Cl-rich (e.g. Candela, 1986). It should be noted, however, that the apatite-fluid partitioning is expected to be a strong function of T and P (Zhu and Sverjensky, 1991).

Whether apatite represents the tail or the dog in halogen mass balance during metamorphism most likely depends on the environment. In high fluid/rock environments where fluid composition controls rock composition (e.g. veins, skarns and ore deposits), apatite composition likely reflects the composition of the infiltrating fluid. In typical regional metamorphic environments where dewatering of fluids and progressive drying out of rocks predominates, apatite likely controls the halogen content of the fluid. For example, consider a rock with ≤1% porosity and 1% modal apatite with a composition $X_F = X_{Cl} = X_{OH} = 1/3$. The fluid composition will be approximately $10^{-5.2}$ m HF and $10^{-2.8}$ m HCl (assuming unit activity of H_2O and ideal mixing). Removal of this fluid and generation of additional H_2O by dewatering of hydrous silicates will progressively deplete the rock in Cl relative to F. Resultant

apatite and coexisting biotite should become increasingly F-rich with progressive dewatering, as indicated by the set of apatite analyses from Kapustin (1987; Fig. 1b).

Smith and Yardley (1999) have applied this type of analysis to the situation in which a Cl-rich detrital apatite is present (Fig. 4a). Their calculations indicate that exchange of Cl with a limited volume of metamorphic fluid can change the concentration of Cl in the fluid by several orders of magnitude.

The partitioning of OH, F, and Cl between apatite and hydrous silicates has also been shown to be temperature sensitive, and has been used as a geothermometer (e.g. Stormer and Carmichael, 1971; Ludington, 1978; Zhu and Sverjensky, 1992; Sallet and Sabatier, 1996; Sallet, 2000). The incorporation of F and Cl into biotite is well-known to be a function of Fe/Mg (e.g. Munoz, 1984), and presumably is also a function of Fe/Mg in apatite (although the total quantities of Fe and Mg in apatite are minor and probably have a negligible affect). Therefore, any thermometer that utilizes the F and Cl content of Fe-Mg silicates must consider this effect. Figure 29 shows a plot from Zhu and Sverjensky (1992) that illustrates the influence of Fe/Mg in biotite on the partitioning of F and Cl between apatite and biotite. Temperature estimates from Figure 29 are quoted as having an uncertainty of 20-40 ˚C (Zhu and Sverjensky, 1992). Conversely, it should be noted that F and Cl in biotite will influence Fe/Mg exchange thermometers involving biotite, and must be accommodated in a fashion such as discussed by Zhu and Sverjensky (1992).

PARAGENESIS OF METAMORPHIC APATITE, MONAZITE AND XENOTIME

There are several mechanisms by which metamorphic phosphates can grow. In the case of monazite this is especially important because recrystallization will reset the Th-U-Pb systematics, and the age measured will be the age of the recrystallization event. Recrystallization can occur by heterogeneous reactions in response to changes in pressure and temperature (prograde or retrograde metamorphism). Recrystallization in shear zones as a result of grain size reduction, influx of fluids and high strain is also possible. Minerals can coarsen by a process such as Ostwald's ripening, possibly enhanced by the presence of a fluid or melt. Growth can occur by intersection with a solvus limb during cooling or by reaching the limits of solubility in a more complex system (e.g. heterogeneous unmixing). Minerals can also be precipitated from a fluid or vapor phase. This section reviews some of the literature pertaining to apatite, monazite, and xenotime recrystallization in metamorphic rocks.

Prograde metamorphism of apatite, monazite and xenotime

Apatite, monazite, and xenotime are found in rocks of nearly every metamorphic grade and, apparently, have wide P-T stability ranges. Despite their widespread occurrence, surprisingly few studies on the prograde metamorphic evolution of phosphates have been published. Kapustin (1987) reported on apatite compositions as a function of metamorphic grade (e.g. Fig. 1b).

Monazite is known to be a detrital mineral, and some low-to-medium grade occurrences of monazite are detrital relics (e.g. Overstreet, 1967; Suzuki and Adachi, 1991; Suzuki et al., 1994; Hawkins and Bowring, 1999; Ferry, 2000; Rubatto et al.,

2001; Wing et al., 2002). Authigenic monazite has been reported from several low-grade occurrences of various bulk compositions. Cabella et al. (2001) reported coexisting monazite and xenotime from pelitic layers in pumpellyite-actinolite facies metacherts (3 kb < P ≤ 4 kb, 300°C < T ≤ 350°C) of the Sestri-Voltaggio zone, Italy. Rasmussen et al. (2001) identified metamorphic monazite in weakly metamorphosed quartz-sericite-chlorite phyllites from the contact aureole of the 1830 Ma Mt. Bundy granite, N. Australia. Overstreet (1967) concluded that, although detrital monazite was not uncommon, monazite is not thermodynamically stable during diagenesis and occurrences of monazite in very low-grade samples were probably detrital relics.

Kingsbury et al. (1993) examined the paragenesis of monazite in a prograde sequence of pelitic schists (unmetamorphosed shale to sillimanite zone) from the eastern Mojave Desert (California, USA). A single detrital grain of monazite was found in the unmetamorphosed shale, along with abundant detrital zircon and apatite and lesser amounts of xenotime and rutile. These authors addressed the issue of stable "sinks" for REEs, Y, Th and U at conditions below monazite appearance. They reported the absence of LREE or Th-bearing phases in unmetamorphosed shales of their study, and suggested that these constituents are located along grain boundaries (adsorbed?) or in clay minerals. In the greenschist facies samples, Kingsbury et al. (1993) reported thorite, thorianite, a possible Ce oxide, and LREE phosphates (not apatite). Monazite was absent from the greenschist facies samples (biotite + chlorite zone) and did not appear until the staurolite zone (T ~ 550 ˚C). Although allanite was not positively identified as a precursor, its former presence was suspected based on the shapes of pseudomorphs. At higher grade (T ~ 650 ˚C) monazite grains were found to

increase in number and to coarsen to their maximum size of approximately 30 μm diameter.

Hawkins and Bowring (1999) reported on the textural development of monazite, xenotime, and titanite from migmatitic gneisses of the Grand Canyon, Arizona. They describe complexly zoned grains with internal truncations of zoning and suggested that solution and redeposition in the presence of a silicate melt was responsible for much of the monazite growth. Additionally, the vestige of monazite cores that record isotopic inheritance was used to infer that the closure temperature of Th-U-Pb is above the peak temperature experienced by these rocks (725 ˚C).

Rubatto et al. (2001) reported on the prograde metamorphism of monazite and zircon from pelitic schists from the Reynolds Range, central Australia. They identified monazite from greenschist-facies samples, which was interpreted to be detrital. Significant growth of new monazite did not occur until the amphibolite facies (sillimanite zone), although no specific reactions were postulated. At the highest grades (granulite facies: Grt + Crd + Bt + Sil + melt), abundant, large monazite grains were found that contain complex internal zoning, suggesting that solution and reprecipitation in the presence of a melt phase was an important mechanism in monazite growth.

Ferry (2000) and Wing et al. (2002) mapped the monazite isograd in three locations: the contact aureole of the Onawa pluton, Maine, the low-P regional Buchan terrane of south-central Maine, and the medium-P Barrovian terrane of central Vermont. Monazite that was characterized as having patchy chemical zoning and irregular habit was found to occur in the lowest grades (chlorite zone) in each terrane, and was interpreted as being detrital. With increasing grade, this monazite was replaced

by allanite, and, very nearly coincident with the Al_2SiO_5 isograd (andalusite in the low-P terranes and kyanite in Vermont), allanite was replaced by monazite. These authors also report that samples with lower than average Al and/or Ca contents contain the low-grade (detrital) monazite rather than allanite to grades as high as the garnet zone, and samples with higher Al and/or Ca contents contain allanite to higher grades than the Al_2SiO_5 isograd.

Pyle and Spear (1999), Pyle et al. (2001), and Pyle (2001) report on the relationship between accessory mineral association (monazite, xenotime, and apatite) and trace element zoning (especially Y and P) in garnet from a suite of pelitic schists of different metamorphic grade from central New England. In these samples, monazite and xenotime are both present in chlorite-biotite zone (garnet-absent) samples, and in the matrix and as inclusions in garnet in samples from the garnet zone. Yttrium contents of garnet from the garnet zone coexisting with xenotime are high (up to several thousand ppm Y), and decrease rapidly with increasing temperature (Pyle and Spear, 2000). Xenotime reacts out continuously as garnet grows, and is typically gone from the matrix assemblage in samples from the middle garnet zone. Monazite grows and displays increasing Y content with increasing T in xenotime-bearing samples, consistent with the monazite-xenotime miscibility gap (Fig. 24). When xenotime reacts out of the assemblage (usually by the middle of the garnet zone), monazite and garnet show a dramatic drop in Y concentration with monazite displaying evidence of continued growth along with garnet. When garnet-consuming reactions are encountered, such as garnet + chlorite + muscovite = staurolite + biotite + H_2O or garnet + chlorite + muscovite = Al_2SiO5 + biotite + H_2O, there is clear textural

evidence that monazite is produced at the expense of garnet, such as the presence of monazite crystals or overgrowths on old crystals in the garnet reaction halo. Monazite was also interpreted to have precipitated in and around leucosomes as melt crystallized.

Phosphates in the melting region

Solubility of phosphates in anatectic melts. The solubility of phosphate is greatest in ultramafic and mafic melts and smallest in granitic melts at identical temperatures and pressures (e.g. Watson, 1979; Ryerson and Hess, 1980). It is also well established that the solubility of apatite in silicate liquids is a strong function of the alumina saturation index (ASI = molar Al/[Na + K + 2Ca]) of the melt (e.g. Bea et al., 1992; Gan and Hess, 1992; Pichivant et al., 1992; Wolf and London, 1994) because of the formation of the aluminum phosphate complex $AlPO_4$. In metaaluminous compositions (ASI = 1), the solubility of apatite is small and dissolved P_2O_5 is less than 0.1 wt% but increases to 0.7 wt% P_2O_5 at ASI = 1.3 (Wolf and London, 1994). Therefore, in metapelitic rocks that contain an Al_2SiO_5 polymorph in the anatectic region in which the ASI is high, the solubility of apatite should likewise be high. For example, using the data of Patiño Douce and Johnston (1991), the ASI of sillimanite-saturated pelitic melts ranges from 1.15 to 1.6, which implies a solubility of P_2O_5 of 0.1 to 1.7 wt% based on the data of Wolf and London (1994). This amount of P_2O_5 is equivalent to the dissolution of 0.3 to over 3.0 modal per cent apatite. If the melt does not leave the rock, the phosphates will precipitate as the melt crystallizes. Apatite solubility is also enhanced in low ASI melts (peralkaline), because of the presence of alkali phosphate complexes (Ellison and Hess, 1988).

In contrast to apatite, the solubilities of monazite and xenotime are much more limited in peraluminous melts compared with apatite solubility, with maximum solubilities of < 0.05 wt% P_2O_5 (Wolf and London, 1995). Indeed, Wolf and London (1995) report precipitation of monazite at sites of apatite dissolution in melting experiments. REE solubilities, in contrast, are higher in mafic compositions relative to granitic compositions (Ryerson and Hess, 1978, 1980), and monazite solubility is greater in peralkaline melts than in meta or peraluminous melts (Montel, 1986, Ellison and Hess, 1988). Rapp and Watson (1986) also report a strong temperature dependence of monazite solubility.

Solubility of phosphates in anatectic melts can be fruitfully analyzed by use of the concept of saturation index (SI) (see also Watt and Harley, 1993). The saturation index is defined as the log of the ratio of the ion activity product (IAP) to the solubility constant (K_{sp}):

$SI = \log (IAP/K_{sp})$

and is a measure of the degree of oversaturation (positive SI) or undersaturation (negative SI) of a mineral. Dissolution of the phosphates apatite, monazite and xenotime into a silicate liquid may be described by the reactions

$Ca_5(PO_4)_3(F) = 5Ca + 3PO_4 + F$ $\quad IAP_{Ap} = (a_{Ca})^5 (a_{PO_4})^3 (a_F)$
apatite

$(LREE)PO_4 = LREE + PO_4$ $\quad IAP_{Mnz} = (a_{LREE})(a_{PO_4})$
monazite

$(Y+HREE)PO_4 = Y + HREE + PO_4$ $\quad IAP_{Xno} = (a_{Y+HREE})(a_{PO_4})$
xenotime

Although simplistic, this approach emphasizes a very important point: phosphate solubility is a function not only of phosphate activity, but the activity of Ca, LREEs, or Y + HREEs as well. Therefore, factors that change the activities of any of these species in the melt will affect the total solubility of the solid.

Complexing in the silicate melt imparts a first-order effect on the activities of melt species. For example, aluminum phosphate complexes, produced by reactions such as

$PO_4 + Al = AlPO_4$,

have the effect of decreasing the activity of PO_4, thus lowering the IAP and SI of apatite resulting in an increase in apatite solubility. Based on this analysis, it is easy to understand why apatite solubility is such a strong function of ASI: the more free Al that is available for production of aluminum phosphate complexes, the more the PO_4 activity will be lowered, thus enhancing apatite solubility. In peralkaline melts, REE phosphate complexes will lower the activity of REEs in the liquid, increasing monazite solubility.

Kinetic considerations. Studies of phosphate solubility reveal kinetic limitations to dissolution rates. Harrison and Watson (1984) and Rapp and Watson (1986) measured the dissolution rates of apatite and monazite, respectively, and found that the dissolution rate is limited by diffusion of P or LREEs away from the dissolving apatite or monazite. Furthermore, the diffusivity, and hence dissolution rate, is strongly dependent on the H_2O content of the melt. In dry melts, dissolution is so slow that complete dissolution of even small crystals of apatite or monazite is unlikely. In melts produced by dehydration melting of muscovite or biotite, where the H_2O content is in the range of 4-8 wt% H_2O, apatite crystals on the order of 500 μm diameter will

dissolve in 100-1000 years. However, monazite dissolution is slower and in a similar melt, a monazite of 50 μm diameter will persist for several million of year at 700 ˚C (Rapp and Watson, 1986), thus making it likely that monazite would survive an anatectic event.

Inferences from studies of natural samples. Considerable evidence exists from natural samples to shed light on the behavior of natural phosphates in the anatectic region. For example, Watt and Harley (1993) examined the geochemistry of two different lower crustal leucogneisses from East Antarctica that were derived from anatexis of pelites, and evaluated the geochemical signatures of each with respect to monazite and apatite reaction with the melt. The geochemistry of one leucogneiss was consistent with little dissolution of accessory phases and removal of melt before complete equilibration. The geochemistry of the other leucogneiss was consistent with accessory phase entrainment resulting from disequilibrium melting. Bea and Montero (1999) examined the geochemistry of host rocks and leucosomes and their major and accessory mineral associations from the Ivrea-Verbano zone, NW Italy. Monazite, apatite, and xenotime were present in samples of kinzigite (incipient migmatites) but their average grain size decreased markedly in the stronolites (high-grade migmatites). Furthermore, the fraction of phosphate crystals contained as inclusions within other minerals (notably garnet) increased dramatically in the stronolites relative to the kinzigites. Xenotime, in particular, was only found as inclusions in garnet in the stronolites, indicating that xenotime consumption occurred as garnet grew. Modal apatite also decreased significantly in stronolites relative to kinzigites. Composition changes were also noted in monazite, notably an increase in the Th/U by a factor of

two. Based on textures, modal changes, and melt composition, Bea and Montero (1999) inferred the melts to have been saturated with respect to apatite and, except at the earliest stages, monazite.

A number of other papers address important aspects of accessory mineral behavior in the melting region, and the reader is encouraged to examine Montel (1993), Dirks and Hand (1991), Miller (1985), Miller and Mittlefehldt, (1982), Watson et al. (1989), Watson and Harrison (1984), Pichavant et al. (1992); Bea, 1996; Bea et al., 1992; and Pyle et al. (2001).

Hydrothermal origin of apatite, monazite and xenotime

The hydrothermal alteration of monazite has received increased attention in recent years in part because of concerns over how alteration will disturb Th-U-Pb systematics and in part because of the proposed application of monazite-like materials as repositories of nuclear waste. Towards this end, Poitrasson et al. (1996) reported on the hydrothermal alteration of monazites from two granites in England, one of which underwent chloritization at T ~ 284 ˚C and the other which underwent greisenization at T ~ 200 ˚C. Chloritization resulted in a leaching of the RE elements, leaving the phosphate framework and the Th-U-Pb systematics intact. Greisenization partially destroyed the phosphate framework, but left the Th concentration intact or even enriched. It was also suggested that the loss of Pb during greisenization might open the possibility of dating the fluid-rock event by $^{207}Pb/^{206}Pb$ *in situ* methods.

Finger et al. (1998) describe hydrothermal alteration of monazite from the eastern Alps. Monazite was replaced by a corona consisting of apatite, allanite, and epidote (outward from monazite). Elements released from monazite (REEs, Y, P, Th and U)

were conserved in the corona, suggesting limited transport by the fluid. Additionally, very little radiogenic Pb was lost from the unaltered part of the monazite, and reasonable crystallization ages were obtained using chemical dating with the electron probe. In contrast, Lanzirotti and Hanson (1996) report on monazite altered to apatite during chloritization that yielded strongly discordant U-Pb ages, suggesting Pb-loss during alteration. Hawkins and Bowring (1997; 1999) and Fitzsimmons et al. (1997) have called upon magmatic fluids as responsible for overgrowths on monazite. Ayers et al. (1999) and Townsend et al. (2000) have suggested that recrystallization during hydrothermal alteration of pre-existing monazite can, in many cases, result in distinctive patchy zoning.

Experimental studies of accessory mineral solubility in aqueous fluids suggests that apatite and monazite solubility in pure H_2O is low, and increases with decreasing pH (Ayers and Watson, 1991). Ayers et al. (1999), in an experimental study of the coarsening kinetics of monazite in the presence of aqueous fluids, found that monazite either recrystallizes and moves as host grain boundaries migrate, or is trapped as inclusions within the host phase. Inclusion monazites, once isolated from the rock matrix, should record the time of entrapment whereas matrix monazite should record the time of final recrystallization, or, if growth zoned, a complex age spectrum.

Implications for monazite and xenotime geochronology

It is clear from the above studies that the accessory minerals monazite, xenotime, and apatite do not behave as an isolated subsystem in metamorphic rocks (e.g. Ferry, 2000; Pyle and Spear, 1999; Pyle et al., 2001). Rather, reactions that involve major phases also affect the amounts and compositions of phosphate minerals. This is so

because phosphorous and REEs exist in phases other than the phosphates, a notable example of which is garnet. Garnet contains up to several hundred ppm P, which can be a considerable fraction of the total P in the rock. For example, consider a rock with 10 modal % garnet with 200 ppm P and 1000 ppm Y, 1 modal % apatite, 0.1 modal % monazite, and 0.01 modal % xenotime (Table 3). Garnet contains only 6% of the total phosphorous budget in this example, similar to xenotime. However, garnet contains 30% of the total Y budget and dominates the mass balance of this element. For this reason, the growth, consumption, and chemical zoning in phosphates clearly is influenced by reactions involving other phases.

The significant consequence of this coupling between the phosphate and silicate minerals in a rock is that the phosphates will grow or be consumed as reactions among the major phases proceed. The simplest observational evidence of this is the nearly ubiquitous zoning observed in the phosphate minerals, especially well represented by monazite. If monazite grew only once during a metamorphic episode it might be systematically zoned from core to rim, but it would never display the complex style of zoning that is observed.

To realize the potential of monazite (and xenotime) as a geochronometer, it is necessary to identify the monazite-producing reactions, and, ideally, to locate them in P-T space. It is clear from the summary above that there are a number of reactions by which monazite may grow during metamorphism, and no simple generalizations are possible.

The first appearance of monazite. The uncertainty surrounding monazite-producing reactions is perhaps best illustrated by the question of what reaction

produces the first appearance of metamorphic monazite. The fact that monazite is sometimes detrital in origin is not in dispute, but the conditions at which the first metamorphic monazite appears are controversial.

In some rocks, metamorphic monazite is clearly preceded by allanite, and the transition from allanite to monazite appears to occur in the middle amphibolite facies (staurolite or Al_2SiO_5 zone) (Overstreet, 1967; Smith and Barreiro, 1990; Kingsbury et al., 1993; Bingen et al., 1996; Harrison et al., 1997; Ferry, 2000; Rubatto et al., 2001; Pyle, 2001; Wing et al., 2002). For the purpose of geochronology, the replacement of allanite by monazite should represent a well-defined metamorphic condition, lending significance to ages determined on such grains (provided inherited cores are not present; Hawkins and Bowring, 1999; Rubatto et al., 2001).

In contrast, several studies have reported what has been interpreted to be metamorphic monazite at grades as low as the chlorite zone, without allanite as a precursor. For example, Franz et al. (1996) report monazite and xenotime from rocks of the chlorite zone in NE Bavaria, and Pyle et al. (2001) report monazite from the chlorite-biotite zone and as inclusions inside garnet from garnet-zone samples in central New England, implying monazite growth in the sub-garnet zone. The precursors to these low-grade monazites are not at all clear. Rhabdophane has been suggested as a precursor to monazite (Sawka et al., 1986), but its instability in the greenschist facies rules out this possibility (Akers et al., 1993). Another possibility is REE enriched clays (e.g. Copeland, et al. 1971), oxides, or hydrous phosphates (e.g. montmorillonite, thorite, thoranite etc.) or Th and REE oxides (Kingsbury et al., 1993).

The range of conditions suggested for the first appearance of monazite during metamorphism (~350-550°C) probably reflects differences in sample bulk compositions and especially the bulk rock Ca (and possibly Al) concentration. In rocks with little or no Ca but some phosphate and REEs, monazite and xenotime appear in the lower greenschist facies because the potential sinks for REEs and Th (clays, thorite, thoranite, LREE oxides, or hydrous phosphates) become unstable at those grades. In rocks with higher Ca (and Al and Ti) content, allanite and possibly titanite apparently harbor the REEs up to the staurolite or Al_2SiO_5 isograds. For example, the rocks examined by Ferry (2000) were calc-pelites and the monazite-in isograd was suppressed to the amphibolite facies. In contrast, the rocks studied by Franz et al. (1996) contained CaO contents of only 0.10 to 0.37 weight per cent, and both monazite and xenotime appeared in the greenschist facies. Significantly, the rocks studied by Kingsbury et al. (1993) were quite low in Ca (0.15-0.39 wt%) and the precursor to monazite was Th- and Ce-oxides rather than allanite. Monazite did not appear until the staurolite zone in these rocks, but the high Al (19.6-24.0 wt%) content of the samples may have stabilized staurolite at a relatively low temperature.

Monazite growth beyond the monazite-in isograd. Once stable, monazite continues to grow, dissolve, and reprecipitate with increasing grade, as evidenced by the complex growth histories recorded in the chemical zoning in many grains. In the sub-solidus, reactions that consume garnet will, in some instances, produce monazite (e.g. Pyle et al., 2001). In the melting region, monazite may dissolve into early formed silicate melt and recrystallize on melt solidification, but the relationships are not well understood (e.g. Hawkins and Bowring, 1999; Rubatto et al., 2001; Pyle et al., 2001).

Hydrothermal fluids also have the potential of causing monazite to precipitate, whether by dissolving and reprecipitating material from existing grains, or by transporting necessary constituents to the deposition site (e.g. Ayers et al., 1999). Formation of shear zones may also induce new monazite growth (e.g. Lanzirotti and Hansen, 1996).

CONCLUDING REMARKS

The past decade has seen an enormous growth of information about metamorphic phosphates. Particularly encouraging is the wealth of information contained in these minerals that is proving extremely useful in deciphering metamorphic histories. These studies point towards a number of fruitful areas for further research:

(1) New studies examining the textures, chemistry, zoning, and petrogenesis of phosphates in well-constrained metamorphic terranes to supplement the current, sparse data sets. Complete, accurate chemical analyses of natural phosphates from these studies would be especially revealing about the geochemical controls on monazite stability.

(2) Additional experimental and empirical studies of the monazite-xenotime miscibility gap including the incorporation of the effects of brabantite substitution ($CaTh(PO_4)_2$) into monazite will further refine the accuracy of this thermometer.

(3) Refinement of the YAG-xenotime and YAG-monazite thermometers to better improve accuracy of calibrations. Currently, these are limited to empirical calibrations from a single metamorphic terrane.

(4) Studies of the incorporation of trace quantities of REEs, P, Th and U into phases other than phosphates will be necessary to better model the interactions between major and accessory phases during metamorphism.

(5) Additional studies on the melting of phosphates will help quantify phosphate solubility and will aid greatly in the interpretation of these minerals from migmatites.

The goal of these studies is to link the paragenesis of these (and other) phases to events in a rock's history which, when combined with texture-sensitive geochronology (e.g. SIMS, LA-ICP-MS, and chemical dating using the electron probe), will enable the determination of the time of these events. These data will allow direct inferences of fundamental tectonic parameters such as the duration of metamorphic events, the duration of melting in the crust, the rates of heating/cooling and burial/exhumation of orogenic belts, and the time and duration of hydrothermal activity.

ACKNOWLDGMENTS

The authors thank Dave Wark for assistance with electron microprobe analysis of complex REE phosphates and E. Bruce Watson for many informative discussions about accessory mineral paragenesis. Careful reviews by L. Storm, G. Franz and J. M. Ferry are also gratefully acknowledged. This work was supported in part by NSF grant EAR-0106738.

REFERENCES

Akers WT, Grove M, Harrison T, Ryerson FJ (1993) The instability of rhabdophane and its unimportance in monazite paragenesis. Chem Geol 110(1-3):169-176

Amli R (1975) Mineralogy and rare earth geochemistry of apatite and xenotime from the Gloserheia granite pegmatite, Froland, southern Norway. Am Mineral 60:607-620

Andrehs G, Heinrich W (1998) Experimental determination of REE distributions between monazite and xenotime: potential for temperature-calibrated geochronology. Chem Geol 149:83-96

Ayres M, Harris N (1997) REE fractionation and Nd-isotope disequilibrium during crustal anatexis from Himalayan leucogranites. Chem Geol 139:249-269

Ayers JC, Miller CF, Gorisch B, Milleman J (1999) Textural development of monazite during high-grade metamorphism: hydrothermal growth kinetics, with implications for U, Th-Pb geochronology. Am Mineral 84:1766-1780

Ayers JC, Watson EB (1991) Solubility of apatite, monazite, zircon, and rutile in supercritical aqueous fluids with implications for subduction zone geochemistry. Phil Trans R Soc Lond 335:365-375

Bea F (1996) Residence of REE, Y, Th, and U in granites and crustal protoliths; implications for the chemistry of crustal melts. J Petrol 37:521-552

Bea F, Fershtater G, Corretge´ LG (1992) The geochemistry of phosphorus in granite rocks and the effect of aluminium. Lithos 29:43-56

Bea F, Montero P (1999) Behavior of accessory phase and redistribution of Zr, REE, Y, Th, and U during metamorphism and partial melting of metapelites in the lower

crust: an example from the Kinzigite Formation of Ivrea-Verbano, NW Italy. Geochim Cosmochim Acta 63:1133-1153

Bea F, Pereira MD, Stroh A (1994) Mineral/leucosome trace-element partitioning in a peraluminous migmatite (a laser ablation-ICP-MS study). Chem Geol 117:291-312

Bingen B, Demaiffe D, Hertogen J (1996) Redistribution of rare earth elements, thorium, and uranium over accessory minerals in the course of amphibolite to granulite facies metamorphism: the role of apatite and monazite in orthogneisses from southwestern Norway. Geochim Cosmochim Acta 60:1341-1354

Brenan JM (1993) Partitioning of fluorine and chlorine between apatite and aqueous fluids at high pressure and temperature: implications for the F and Cl content of high P-T fluids. Earth Planet Sci Lett 117:251-263

Cabella R, Lucchetti G, Marescotti P (2001) Authigenic Monazite and xenotime from pelitic metacherts in pumpellyite-actinolite-facies conditions, Sestri-Voltaggio Zone, central Liguria, Italy. Can Mineral 39:717-727

Candela PA (1986) Towards a thermodynamic model for the halogens in magmatic systems - an application to melt vapour apatite equilibria. Chem Geol 57:289-301

Catlos EJ, Harrison TM, Kohn MJ, Grove M, Ryerson FJ, Manning CE, Upreti BN (2001) Geochronologic and thermobarometric constraints on the evolution of the Main Central Thrust, central Nepal Himalaya. J Geophys Res 106:16177-16204

Cherniak DJ (2001) Rare earth element diffusion in apatite. Geochim Cosmochim Acta 64:3871-3885

Cherniak DJ, Watson EB, Harrison TM, Grove M (2000) Pb diffusion in monazite: a progress report on a combined RBS/SIMS study. EOS Trans Am Geophys Union 41:S25

Copeland RA, Frey FA, Wones DR (1971) Origin of clay minerals in a mid-Atlantic ridge sediment. Earth Planet Sci Lett 10:186-192

Crowley JL, Ghent ED (1999) An electron microprobe study of the U-Pb-Th systematics of metamorphosed monazite: the role of Pb diffusion versus overgrowth and recrystallization. Chem Geol 157:285-302

Cruft EF (1966) Minor elements in igneous and metamorphic apatite. Geochim Cosmochim Acta 30:375-398

Dirks P, Hand M (1991) Structural and metamorphic controls on the distribution of zircon in an evolving quartzofeldspathic migmatite: an example from the Reynolds Range, central Australia. J Metamorph Geol 9:191-201

Ellison AJG, Hess PC (1988) Peraluminous and peralkaline effects upon "monazite" solubility in high-silica liquids. EOS Trans Am Geophys Union 69:498

Ferry JM (2000) Patterns of mineral occurrence in metamorphic rocks. Am Mineral 85:1573-1588

Finger F, Broska I, Roberts MP, Schermaier A (1998) Replacement of primary monazite by apatite-allanite-epidote coronas in an amphibolite facies granite gneiss from the eastern Alps. Am Mineral 83:248-258

Fitzsimmons ICW, Kinny PD, Harley SL (1997) Two stages of zircon and monazite growth in anatectic leucogneiss; SHRIMP constraints on the duration and intensity of Pan-African metamorphism in Prydz Bay, east Antarctica. Terra Nova 9:47-51

Förster H-J (1998) The chemical composition of REE-Y-Th-U-rich accessory minerals in peraluminous granites of the Erzgebirge-Fichelgebirge region, Germany, part I: The monazite-(Ce)-brabantite solid solution series. Am Mineral 83:259-272

Foster G, Kinny P, Vance D, Prince C, Harris N (2000) The significance of monazite U-Pb-Th age data in metamorphic assemblages; a combined study of monazite and garnet chronometry. Earth Planet Sci Lett 181:327-340

Franz G, Andrehs G, Rhede D (1996) Crystal chemistry of monazite and xenotime from Saxothuringian-Moldanubian metapelites, NE Bavaria, Germany. Eur J Mineral 8:1097-1108

Gan H, Hess PC (1992) Phosphate speciation in potassium aluminosilicate glass. Am Mineral 77:495-506

Görz H, White EH (1970) Minor and trace elements in HF-soluble zircons. Contrib Mineral Petrol 29:180-182

Gratz R, Heinrich W (1997) Monazite-xenotime thermobarometry: experimental calibration of the miscibility gap in the system $CePO_4$-YPO_4. Am Mineral 82:772-780

Gratz R, Heinrich W (1998) Monazite-xenotime thermometry, III; experimental calibration of the partitioning of gadolinium between monazite and xenotime. Eur J Mineral 10:579-588

Grauch RI (1989) Rare earth elements in metamorphic rocks. Rev Mineral 21: 147-167

Harrison TM, Ryerson FJ, Le Fort P, Yin A, Lovera OM, Catlos EJ (1997) A Late Miocene-Pliocene origin for the Central Himalayan inverted metamorphism. Earth Planet Sci Lett 146:1-7

Harrison TM, Watson EB (1984) The behavior of apatite during crustal anatexis: equilibrium and kinetic considerations. Geochim Cosmochim Acta 48:1467-1477

Hawkins DP, Bowring SA (1997) U-Pb systematics of monazite and xenotime: case studies from the Paleoproterozoic of the Grand Canyon, Arizona. Contrib Mineral Petrol 127:87-103

Hawkins DP, Bowring SA (1999) U-Pb monazite, xenotime, and titanite geochronological constraints on the prograde to post-peak metamorphic thermal history of Paleoproterozoic migmatites from the Grand Canyon, Arizona. Contrib Mineral Petrol 134:150-169

Heinrich W, Andrehs G, Franz G (1997) Monazite-xenotime miscibility gap thermometry. I. An empirical calibration. J Metamorph Geol 15:3-16

Jamtveit B, Dahlgren S, Austrheim H (1997) High-grade contact metamorphism of calcareous rocks from the Oslo Rift, southern Norway. Am Mineral 82:1241-1254

Kapustin YL (1987) The composition of apatite from metamorphic rocks. Geochem Int'l 24:45-51

Kingsbury JA, Miller CF, Wooden JL, Harrison TM (1993) Monazite paragenesis and U-Pb systematics in rocks of the eastern Mojave Desert, California, USA: implications for thermochronometry. Chem Geol 110: 147-167

Korzhinskiy MA (1981) Apatite solid solutions as indicators of the fugacity of HCl and HF in hydrothermal fluids. Geochem Int'l 3:45-60

Lanzirotti A, Hanson GN (1996) Geochronology and geochemistry of multiple generations of monazite from the Wepawaug Schist, Connecticut, USA;

implications for monazite stability in metamorphic rocks. Contrib Mineral Petrol 125:332-340

Lee DE, Bastron H (1967) Fractionation of rare-earth elements in allanite and monazite as related to geology of the Mt. Wheeler mine area, Nevada. Geochim Cosmochim Acta 31:339-356

Liou JG, Zhang RV, Ernst WG, Rumble DI, Maruyama S (1998) High-pressure minerals from deeply subducted metamorphic rocks. Rev Mineral 37: 33-96

Ludington S (1978) The biotite-apatite geothermometer revisited. Am Mineral 63:551-553

Miller CF (1985) Are strongly peraluminous magmas derived from pelitic sedimentary sources? J Geol 93:673-689

Miller CF, Mittlefehldt DW (1982) Depletion of LREE in felsic magmas. Geol 10:129-133

Montel J-M (1986) Experimental determination of the solubility of Ce-monazite in SiO_2-Al_2O_3-K_2O-Na_2O melts at 800°C, 2 kbar, under H_2O-saturated conditions. Geol 14:659-662

Montel J-M (1993) A model for monazite/melt equilibrium and application to the generation of granitic magmas. Chem Geol 110:127-146

Munoz JL (1984) F-OH and Cl-OH exchange in micas with applications to hydrothermal ore deposits. Rev Mineral 13:469-493

Nijland TG, Jansen JBH, Maijer C (1993) Halogen geochemistry of fluid during amphibolite-granulite metamorphism as indicated by apatite and hydrous silicates in basic rocks from the Bamble sector, South Norway. Lithos 30:167-189

Overstreet WC (1967) The geologic occurrence of monazite. U.S. Geological Survey Professional Paper 530, Washington, D. C.

Parrish R (1990) U-Pb dating of monazite and its application to geological problems. Can J Earth Sci 27:1431-1450

Patiño Douce AE, Johnston AD (1991) Phase equilibria and melt productivity in the pelitic system: implications for the origin of peraluminous granitoids and aluminous granulites. Contrib Mineral Petrol 107:202-218

Pichavant M, Montel J-M, Richard LR (1992) Apatite solubility in peraluminous liquids: experimental data and an extension of the Harrison-Watson model. Geochim Cosmochim Acta 56:3855-3861

Poitrasson F, Chenery SR, Bland DJ (1996) Contrasted monazite hydrothermal alteration mechanisms and their geochemical implications. Earth Planet Sci Lett 145:79-96

Poitrasson F, Chenery SR, Shepherd TJ (2000) Electron microprobe and LA-ICP-MS study of monazite hydrothermal alteration: implications for U-Th-Pb geochronology and nuclear ceramics. Geochim Cosmochim Acta 64:3283-3297

Puchelt H, Emmermann R (1976) Bearing of rare earth patterns of apatites from igneous and metamorphic rocks. Earth Planet Sci Lett 31:279-286

Pyle JM (2001) Distribution of select trace elements in pelitic metamorphic rocks: pressure, temperature, mineral assemblage, and reaction-history controls. PhD Dissertation, Rensselaer Polytechnic Institute, Troy, New York

Pyle JM, Spear FS (1999) Yttrium zoning in garnet: coupling of major and accessory phases during metamorphic reactions. Geol Mat Res 1:1-49

Pyle JM, Spear FS (2000) An empirical garnet (YAG) - xenotime thermometer. Contrib Mineral Petrol 138:51-58

Pyle JM, Spear FS, Rudnick RL, McDonough WF (2001) Monazite–Xenotime–Garnet Equilibrium in Metapelites and a New Monazite–Garnet Thermometer. J Petrol 42:2083-2107

Rapp RP, Watson EB (1986) Monazite solubility and dissolution kinetics; implications for the thorium and light rare earth chemistry of felsic magmas. Contrib Mineral Petrol 94:304-316

Rasmussen B, Fletcher IR, McNaughton NJ (2001) Dating low-grade metamorphic events by SHRIMP U-Pb analysis of monazite in shales. Geol 29:963-966

Romans PA, Brown LL, White JC (1975) An electron microprobe study of yttrium, rare earth, and phosphorus distribution in zoned and ordinary zircon. Am Mineral 60:475-480

Rubatto D, Williams IS, Buick IS (2001) Zircon and monazite response to prograde metamorphism in the Reynolds Range, central Australia. Contrib Mineral Petrol 140:458-468

Ryerson FJ, Hess PC (1978) Implications of liquid-liquid distribution coefficients to mineral-liquid partitioning. Geochim Cosmochim Acta 42:921-932

Ryerson FJ, Hess PC (1980) The role of P_2O_5 in silicate melts. Geochim Cosmochim Acta 44:611-624

Sallet R (2000) Fluorine as a tool in the petrogenesis of quartz-bearing magmatic associations: applications of an improved F-OH biotite-apatite thermometer grid. Lithos 50:241-253

Sallet R, Sabatier H (1996) A new formulation of the biotite-apatite geothermometer. Applications to magmatic and sub-solidus conditions: Santa Catarina, Brazil, and Bingham, USA mining districts; Bishop Tuff, USA and Ploumanac'h granite, France. Sociedade Brasileira de Geologia, 39° Congresso Brasileiro de Geologia, 2:115-119

Sawka WN, Banfield JF, Chappell BW (1986) A weathering-related origin of widespread monazite in S-type granites. Geochim Cosmochim Acta 50:171-175

Seydoux-Guillaume A-M, Wirth R, Heinrich W, Montel J-M (in press) Experimental determination of thorium partitioning between monazite and xenotime using analytical electron microscopy. Eur J Mineral

Sisson VB (1987) Halogen chemistry as an indicator of metamorphic fluid interaction with the Ponder Pluton, Coast Plutonic Complex, British Columbia, Canada. Contrib Mineral Petrol 95:123-131

Smith HA, Barreiro B (1990) Monazite U-Pb dating of staurolite grade metamorphism in pelitic schists. Contrib Mineral Petrol 105:602-615

Smith HA, Giletti BJ (1997) Lead diffusion in monazite. Geochim Cosmochim Acta 61:

Smith MP, Yardley BWD (1999) Fluid evolution during metamorphism of the Otago Schist, New Zealand; (II), Influence of detrital apatite on fluid salinity. J Metamorph Geol 17:187-193

Stormer JC, Carmichael ISE (1971) Fluorine-hydroxyl exchange in apatite and biotite: A potential igneous geothermometer. Contrib Mineral Petrol 31:121-131

Stormer JCJ, Pierson MJ, Tacker RC (1993) Variation of F and Cl X-ray intensity due to anisotropic diffusion of apatite during electron microprobe analysis. Am Mineral 78:641-648

Suzuki K, Adachi M (1991) Precambrian provenance and Silurian metamorphism of the Tsubonosawa paragneiss in the south Kitakami terrane, northeast Japan, revealed by the chemical Th-U-total Pb isochron ages of monazite, zircon and xenotime. Geochem J 25:357 - 376

Suzuki K, Adachi M, Kajizuka I (1994) Electron microprobe observations of Pb diffusion in metamorphosed detrital monazites. Earth Planet Sci Lett 128:391-405

Terry MP, Robinson P, Hamilton MA, Jercinovic MJ (2000) Monazite geochronology of UHP and HP metamorphism, deformation, and exhumation, Nordøyane, Western Gneiss Region, Norway. Am Mineral 85:1651-1664

Townsend KJ, Miller CF, D'Andrea JL, Ayers JC, Harrison TM, Coath CD (2000) Low temperature replacement of monazite in the Ireteba granite, southern Nevada: geochronological implications. Chem Geol 172:95-112

Viskupic K, Hodges KV (2001) Monazite-xenotime thermochronometry: methodology and an example from the Nepalese Himalaya. Contributions to Mineralogy and Petrology 141:233-247

Watson EB (1979) Apatite saturation in basic to intermediate magmas. Geophys Res Lett 6:937-940

Watson EB (1980) Apatite and phosphorus in mantle source regions: an experimental study of apatite/melt equilibria at pressures to 25 kbar. Earth Planet Sci Lett 51:322-335

Watson EB, Capobianco CJ (1981) Phosphorus and the rare earth elements in felsic magmas: an assessment of the role of apatite. Geochim Cosmochim Acta 45:2349-2358

Watson EB, Harrison TM (1984) What can accessory minerals tell us about felsic magma evolution?: A framework for experimental study. Proc 27th Int'l Cong 11:503-520

Watson EB, Vicenzi EP, Rapp RP (1989) Inclusion/host relations involving accessory minerals in high-grade metamorphic and anatectic rocks. Contrib Mineral Petrol 101:220-231

Watt GL, Harley SL (1993) Accessory phase controls on the geochemistry of crustal melts and restites produced during water-undersaturated partial melting. Contrib Mineral Petrol 114:550-566

Williams ML, Jercinovic MJ, Terry MP (1999) Age mapping and dating of monazite on the electron microprobe; deconvoluting multistage tectonic histories. Geol 27:1023-1026

Wing BA, Ferry JM, Harrison TM (2002) Prograde destruction and formation of monazite and allanite during contact and regional metamorphism of pelites: petrology and geochronology. Contrib Mineral Petrol

Wolf MB, London D (1994) Apatite dissolution into peraluminous haplogranitic melts: An experimental study of solubilities and mechanisms. Geochim Cosmochim Acta 58:4127-4145

Wolf MB, London D (1995) Incongruent dissolution of REE- and Sr- rich apatite in peraluminous granitic liquids: Differential apatite, monazite, and xenotime solubilities during anatexis. Am Mineral 80:765-775

Yang P, Rivers T (2002) Trace element zoning in pelitic garnet, apatite and epidote group minerals: The origin of Y annuli and P zoning in garnet. Geol Mat Res 4:1-35

Yardley BWD (1985) Apatite composition and fugacities of HF and HCl in metamorphic fluids. Mineral Mag 49:77-79

Zayats AP, Kuts VP (1964) Rare earth elements in the accessory minerals of gneisses in the Ukrainian crystalline shield. Geochem Int'l 1:1126-1128

Zhu C, Sverjensky DA (1991) Partitioning of F-Cl-OH between minerals and hydrothermal fluids. Geochim Cosmochim Acta 55:1837-1858

Zhu C, Sverjensky DA (1992) F-Cl-OH partitioning between biotite and apatite. Geochim Cosmochim Acta 56:3435-3467

Zhu XK, O'Nions RK (1999a) Zonation of monazite in metamorphic rocks and its implications for high temperature thermochronology: a case study from the Lewisian terrain. Earth Planet Sci Lett 171:209-220

Zhu XK, O'Nions RK (1999b) Monazite chemical composition: some implications for monazite geochronology. Contrib Mineral Petrol 137:351-363

Table 1: Ranked Textural and Compositional Criteria for Assumption of Monazite-Xenotime Compositional Equilibrium. From Pyle et al. (2001)

Observed textural and/or compositional criteria	Assumption	Relative rank
Physical contact of monazite and xenotime grains	Both grains in compositional equilibrium	1
Y-homogeneous monazite and xenotime coexist in sample matrix (not necessarily in contact)	All matrix monazite and xenotime in equilibrium	2
Y-homogenous monazite and xenotime included in same garnet, with no garnet yttrium discontinuities between the two inclusions	Included monazite and xenotime in equilibrium	3
Discontinuously Y-zoned monazite and xenotime coexist in sample matrix (not necessarily in contact)	Only high-Y portion of monazite in equilibrium with xenotime	4
Discontinuously Y-zoned monazite and xenotime included in same garnet, with no garnet yttrium discontinuities between the two inclusions	Only high-Y portion of monazite in equilibrium with xenotime	5
Discontinuously Y-zoned monazite included in specific garnet, and xenotime included in different grain of garnet, and both inclusions present in same type of "compositional domain" within garnets	Only high-Y portion of monazite in equilibrium with xenotime	6
Discontinuously Y-zoned monazite included in garnet, and xenotime present in matrix	Only high-Y portion of monazite in equilibrium with xenotime	7
Monazite and some portion of occluding garnet are approximately homogeneous in Y, and monazite Y content is comparable to that of monazite in xenotime-bearing samples of the same metamorphic grade	Monazite grew with xenotime present in the mineral assemblage (now absent?)	8

Table 2: Ranked Textural and Compositional Criteria for Assumption of Monazite-Garnet Compositional Equilibrium. From Pyle et al. (2001)

Observed textural and/or compositional criteria	Assumption	Relative rank
Inclusion of homogeneous monazite in homogeneous or continuously Y-zoned garnet	Both grains in (compositional) equilibrium	1
Discontinuously Y-zoned monazite included in homogeneous or continuously Y-zoned garnet	Garnet in equilibrium with outer portion of monazite	2
Matrix monazite and garnet both homogeneous or continuously Y-zoned	Both grains in equilibrium	3
Garnet homogeneous or continuously Y-zoned; matrix monazite discontinuously Y-zoned	Garnet in equilibrium with outer portion of monazite	4
Garnet discontinuously Y-zoned, included monazite discontinuously Y-zoned	None: knowledge of reaction relationship needed	--
Garnet discontinuously Y-zoned; matrix monazite discontinuously Y-zoned	None: knowledge of reaction relationship needed	--
Textural evidence for monazite-garnet reaction relationship	Monazite and portion of garnet involved in reaction in equilibrium if reaction produces both phases	Used in conjunction with all of above

Table 3. Mass balance calculations for P and Y

	density	mode	grams phase	wt% P	total gm P	% mass of P	wt % Y	total gm Y	% mass of Y
Garnet	4.2	10	42	0.02	0.840	6.0	0.1	4.2	29.9
Apatite	3.2	0.1	0.32	18.452	5.904	42.1	0.2	0.064	0.5
Xenotime	4.5	0.01	0.045	16.939	0.762	5.4	48	2.16	15.4
Monazite	5	0.1	0.5	13.044	6.522	46.5	1	0.5	3.6

FIGURE CAPTIONS

Figure 1. (a) Ternary F-OH-Cl plot of metamorphic apatite compositions from pelites from central New England, USA (from Pyle, 2001). (b) Compositions of metamorphic apatite separated by metamorphic grade. Note that maximum Cl content decreases and F/(F+OH) increases with metamorphic grade. Data from Kapustin (1984).

Figure 2. Plots showing compositions of metamorphic apatite from pelites from central New England (data from Pyle, 2001). Units are cations/8 oxygens. (a) Fe; (b) Mg; (c) Mn; (d) Fe-Mg-Mn ternary plot; (e) Y; and (f) ∑LREEs (La-Sm).

Figure 3. REE plots of apatite (a, d), monazite (b, e) and xenotime (c, f). REE plots in a, b, and c are from sources indicated and represent a restricted suite of rock compositions (taken from Grauch, 1989). REE plots in d, e, and f are compilations of analyses from the literature and show a wider total spread of values. Lined fields in d, e, and f encompass all tabulated analyses. Stippled fields in e and f are the same data with suspected spurious points eliminated. Data on monazite and xenotime from Pyle (2001); Franz et al. (1996), Finger et al. (1998), Förster (1998), and Zhu and O'Nions (1999b). Data for apatite from Bea and Montero (1999), Finger et al. (1998), Bingen et al. (1996), Amli (1975), Jamtveit et al. (1997), Bea

(1996), Lee and Bastron (1967), Puchelt and Emmerman (1976), Ayers and Harris (1997), Cruft (1996), and Pyle (2001).

Figure 4. Zoning in metamorphic apatite. (a) Detrital Cl-rich apatite core and F-rich low-grade (pumpellyite-actinolite facies) metamorphic overgrowth. From Smith and Yardley (1999). (b) Zoned metamorphic apatite from Yang and Rivers (2002). Bright areas correspond to higher Y concentrations. Overlay of dots connected by lines show traverse analyzed for Y concentration. (c) F and (d) Fe/(Fe+Mg) zoning in apatite from leucosome, west-central New Hampshire (Pyle, unpublished data).

Figure 5. Backscatter electron (BSE) images and X-ray composition maps of metamorphic xenotime textures. (a) X-ray map of Y concentration in garnet from eastern Vermont showing high Y in the core where xenotime inclusions are located (white spots in garnet core) and low Y elsewhere. (b) Yttrium X-ray composition map of garnet in from staurolite grade pelite from New Hampshire. Note truncation of high-Y annulus and three xenotime crystals (three white dots) where annulus is truncated on lower garnet rim. (c) BSE image of lower corner of (b) showing xenotime grains located in the relict annulus (dotted lines). (d) Xenotime formed along grain-boundaries of late generation apatite grains occurring in leucosomes, migmatite zone, west-central New Hampshire. Numbers on images are Y concentration in ppm. Grt = garnet; Bt = biotite; Mnz = monazite; Xno = xenotime; Ap = apatite; Plg = plagioclase; Qtz = quartz; Zrn = zircon; Ilm = ilmenite; Py = pyrite. From Pyle and Spear (1999) and Pyle (2001).

Figure 6. Histograms of monazite compositions (cations/4 oxygens). (a) Ce, (b) Nd, (c) La, (d) Y, (e) ∑HREEs (Gd-Lu). Note the restricted range of composition displayed for LREEs. Data sources as in Figure 3.

Figure 7. Histograms of xenotime compositions (cations/4 oxygens). (a) Y, (b) Gd, (c) Dy, (d) Er, (e) Yb. Most metamorphic xenotimes are 75-80% YPO_4 with limited ranges of HREEs. Data sources as in Figure 3.

Figure 8. Ternary plots of (a) monazite and (b,c) xenotime compositions. Note restricted range of monazite compositions, plus the nearly constant Ce values. Note the strong correlation in xenotime (b) between Dy and Yb. Data sources as in Figure 3.

Figure 9. Histograms of Th and U concentrations in metamorphic (a,b) monazite and (c,d) xenotime. (a) Metamorphic monazites have average Th concentrations of 0.03-0.05 cations/4 oxygens, although maximum values are over 0.25 atoms/4 oxygens. (b) U values in monazite are typically less than 0.005 cations/4 oxygens. Xenotime Th and U values are generally smaller than those in monazite. Note the difference in Th scales between monazite (a) and xenotime (c). Data sources as in Figure 3.

Figure 10. Ternary plots of metamorphic monazite and xenotime analyses from the literature. (a) LREE-HREE-Y in monazite; (b) LREE-Th+U-HREE+Y in monazite;

(c) LREE-HREE-Y in xenotime; (d) LREE-Th+U-HREE+Y in xenotime. Data sources as in Figure 3.

Figure 11. Plots of monazite composition illustrating chemical exchanges. (a) Th + U versus Si + Ca. The strong linear trend suggests that most Th + U is accommodated by a combination of the brabantite ($(Th,U)Ca(PO_4)_2$) and huttonite ($(Th,U)SiO_4$) exchanges. (b) Th + U versus Ca. (c) Th + U versus Si. The strong correlation of Th + U with Ca in (b) suggests the brabantite exchange dominates in metamorphic monazite. (d) Th + U – Si. (e) Th + U – Ca. These "residual" plots show the amount of Th + U that is charge compensated by either Ca (d) or Si (e). Data sources as in Figure 3.

Figure 12. Plots of xenotime composition illustrating chemical exchanges. (a) Th + U versus Si + Ca. (b) Th + U versus Ca. (c) Th + U versus Si. The lack of a strong correlation of Th + U with Si, Ca or Si + Ca suggests that additional elements must be considered in the charge compensation of metamorphic xenotime. The most likely candidate is Zr component in xenotime, which would be compensated by Si in a "zircon" molecule ($ZrSiO_4$). Unfortunately, few analyses of metamorphic xenotime include analyses for Zr. Data sources as in Figure 3.

Figure 13. BSE images and chemical zoning profiles of monazite from Zhu and O'Nions (1999a) showing three major types of zoning observed. (a) Simple concentric zoning. (b, c) Complex concentric zoning. (d) intergrowth zoning. (e)

Patchy zoning. (f) Composition profiles of the monazite in (b) along the line A-B. (g) Composition profiles of the monazite in (c) along the line A'-B'. Note the sympathetic zoning of Pb with Th and U and Si + Ca with Th and U. Also note the sharp gradients in all elements indicating very little diffusional relaxation.

Figure 14. X-ray maps showing chemical zoning in a monazite from Nepal, central Himalaya. (a) Th; (b) Si; (c) U; and (d) Y. Note the sympathetic zoning of Th and Si and, to a lesser degree, U. Y zoning is similar, but not as sharp. (M. Kohn, unpublished data).

Figure 15. Images showing compositional zoning in metamorphic monazite. (a, d, g, j) BSE images; (b, e, h, k) Y distribution maps; (c, f, i, l) Th distribution maps. Brighter areas indicates higher concentration of element. (a-c) Monazite from the garnet zone of eastern Vermont. Y is roughly homogeneous, and Th decreases towards the monazite rim, corresponding with back-scatter zoning. (d-f) Monazite from the sillimanite zone, west-central New Hampshire. Back-scatter brightness corresponds to Th enrichment, and Y zoning is antithetic to Th zoning. (g-i) Monazite from the transitional sillimanite/migmatite zone, west-central New Hampshire. Th is nearly homogeneous, but Y is complexly zoned (corresponding to back-scatter variation), with at least four distinct compositional zones visible in the map. (j-l) Monazite from cordierite + garnet migmatites, central New Hampshire. High Y rim on left of grain is monazite crystallized from melt. Three zones of

intermediate Y concentration were produced during prograde metamorphism. The high Th core may be a detrital relict. From Pyle et al. (2001) and Pyle (2001).

Figure 16. (a,b) Cartoon depicting complex monazite growth geometry (a) and resulting 2-D image from arbitrary thin section cut through the grain (b). Only two monazite compositional zones are present in (a), but the zoning observed in the cut through the complex geometry could be misinterpreted as four growth zones (b). (c) Yttrium X-ray maps of monazites with complex internal zoning (same sample as Fig. 15g-i) showing two to four growth zones, supporting the interpretation that crystals displaying four growth zones are the result of the orientation of the thin section cut through a complex geometry. From Pyle (2001).

Figure 17. BSE images of xenotime showing complex internal geometries. (a) Xenotime from Nepal, Himalaya (from Viskupic and Hodges, 2001). (b,c) Xenotimes from kyanite metaquartzite, New Mexico (from C. Daniel and J. Pyle, unpublished data).

Figure 18. X-ray composition maps of xenotime (Fig. 17b) showing complex internal zoning. Y and Yb are antithetic, and P zoning reflects change in average atomic weight sympathetic to Y, Yb and Dy substitutions. Zoning of Si and U are sympathetic, indicative of U + Si = REE + P substitution and are apparently decoupled from Y, Yb and Dy zoning. Th, Zr, Pb and Ca do not display observable

zoning in this grain. Comparison with Fig. 17b reveals that BSE contrast is due to variations in Y+HREEs. (From C. Daniel and J. Pyle, unpublished data).

Figure 19. Age zoning in monazite. (a-d) Monazite from Western Gneiss Region, Norway, shows complex internal zoning in Th (a) and U (b), but only two age domains (c and d). Age traverse in (d) taken from core (right) to rim (left). From Williams et al. (1999). (e) BSE image and (f) chemical and age zoning in monazite from the Monashee complex, British Columbia, Canada. Concentrically zoned core (e) of monazite shows variation in Th and Pb, but little age variation. Rim, which displays a composition similar to the near-rim, is considerably younger than the bulk of the grain. From Crowley and Ghent (1999).

Figure 20. Schematic representation of the four possible combinations of garnet and monazite reaction relationships and the implications of these for finding equilibrated garnet-monazite pairs. At the left in each panel: Solid outlines show grain boundary positions at time 1 (t_1). At the right in each panel: Solid lines show grain positions at time 2 (t_2), and dashed lines show former (t_1) grain boundary positions. Garnet and monazite are assumed to be in equilibrium at t_1, and both are assumed to be refractory (zoned) phases. (a) Garnet and monazite both grow between t_1 and t_2. The grain boundary of included monazite is in equilibrium with some portion of the occluding garnet between the monazite-garnet grain boundary and the garnet-matrix grain boundary. Rim of matrix monazite is in equilibrium with rim of garnet. (b) Garnet grows and monazite is consumed between t_1 and t_2.

(c) Garnet is consumed and monazite grows between t_1 and t_2. (d) Garnet and monazite both consumed between t_1 and t_2. In (b), (c), and (d), no existing portion of garnet is in equilibrium with monazite. From Pyle et al. (2001).

Figure 21. Plot of $\log(K_D)$(monazite/xenotime) for coexisting monazite-xenotime pairs from NE Bavaria, Germany. Modified from Franz et al. (1996).

Figure 22. Composition plots of coexisting monazite and xenotime. (a) LREE – HREE - Y ternary showing tie lines between coexisting monazite and xenotime. (b) LREE - HREE+Y – (Th+U+Pb) ternary. X = biotite + chlorite zone, squares = garnet zone, triangles = staurolite zone, circles = sillimanite zone, diamonds = migmatite zone. From Pyle et al. (2001).

Figure 23. Plots of average $K_{eq} = (Y/(Gd,Dy))_{Mnz}/(Y/(Gd,Dy))_{Xno}$ vs. metamorphic grade. Error bars represent ±1 standard deviation on the average value of K_{eq} for each metamorphic zone. Number of monazite analyses averaged per zone is as follows: Bt-Chl (28); Grt (97), St (120), Sil (123), Mig (88). From Pyle et al. (2001).

Figure 24. Monazite-xenotime miscibility gap. (a) Experimental data from Gratz and Heinrich (1997). (b) Experimental and natural monazite-xenotime pairs from Heinrich et al. (1997) and Andrehs and Heinrich (1998). Note the X axis here is Y + HREEs. (b) Natural coexisting monazite and xenotime from Pyle et al. (2001). (d)

The effect of Th+Si substitution in monazite on the miscibility gap (Seydoux-Guillaume et al., 2002).

Figure 25. Ternary ($CePO_4$-YPO_4-$ThSiO_4$) plots showing the stability fields for monazite, xenotime and thorite as a function of temperature (Seydoux-Guillaume et al., 2002).

Figure 26. YAG – Xenotime thermometer. (a) P-T plot of eleven garnet yttrium analyses from nine xenotime-bearing pelites showing empirical P-T dependence of garnet YAG composition coexisting with xenotime. Labels indicate concentration of Y in garnet (ppm). Lines are contours of Y concentration in garnet (ppm) drawn by inspection. (b) Plot of ln(ppm Y in garnet) vs. reciprocal absolute temperature for xenotime-bearing pelites. Error bars represent assumed accuracy measurements on temperature estimates from thermobarometry (± 30°C) and electron microprobe measurements of garnet composition (± 100 ppm Y). (c) Graphical representation of the garnet-xenotime thermometer as a plot of garnet composition (ppm Y in garnet) vs. calculated temperature, using the regression from (b). Bars show precision of temperature estimate at different Y concentrations assuming $\sigma_{[Y]_{Grt}}$ = ± 100 ppm. From Pyle and Spear (2000).

Figure 27. Plot of $\ln(K_{Eq}) + P\Delta V_s/RT$ vs. reciprocal temperature for the reaction YAG + OH-apatite + 25/4 quartz = 5/4 grossular + 5/4 anorthite + 3 YPO_4 monazite + 1/2 H_2O. Solid squares = xenotime-bearing assemblages, open squares = xenotime-

absent assemblages. Least squares regression line is fit to all data points. Horizontal error bars represent temperature uncertainty of ±30°C. Vertical error bars are ±1σ (ln K_{Eq} + PΔV/RT), derived from propagation of uncertainties in P (± 1000 bars), T (±30°C), ΔV_{rxn} (1%), compositional parameters (0.001 mole fraction YAG, 0.01 mole fraction all others), and $f(H_2O)$ (±7.5; 1000 trial Monte Carlo simulation). Labels on graph indicate sample numbers. From Pyle et al. (2001).

Figure 28. Apatite-fluid partitioning. (a) Plot of logs of activity ratios (HF/H_2O versus HCl/H_2O) in fluid with composition fields of apatite indicated. From Zhu and Sverjensky (1991). (b-d) Isopleths showing mole fractions of apatite components calculated from data in (a) and assuming ideal mixing. Note that high concentrations of F-apatite are possible in fluids considerably more dilute in HF than is the case for Cl-apatite.

Figure 29. Plot of T versus $\ln K_{eq}$ for coexisting biotite and apatite. Note the strong dependence of K_{eq} on the Fe/(Fe+Mg) of biotite. From Zhu and Sverjensky (1992).

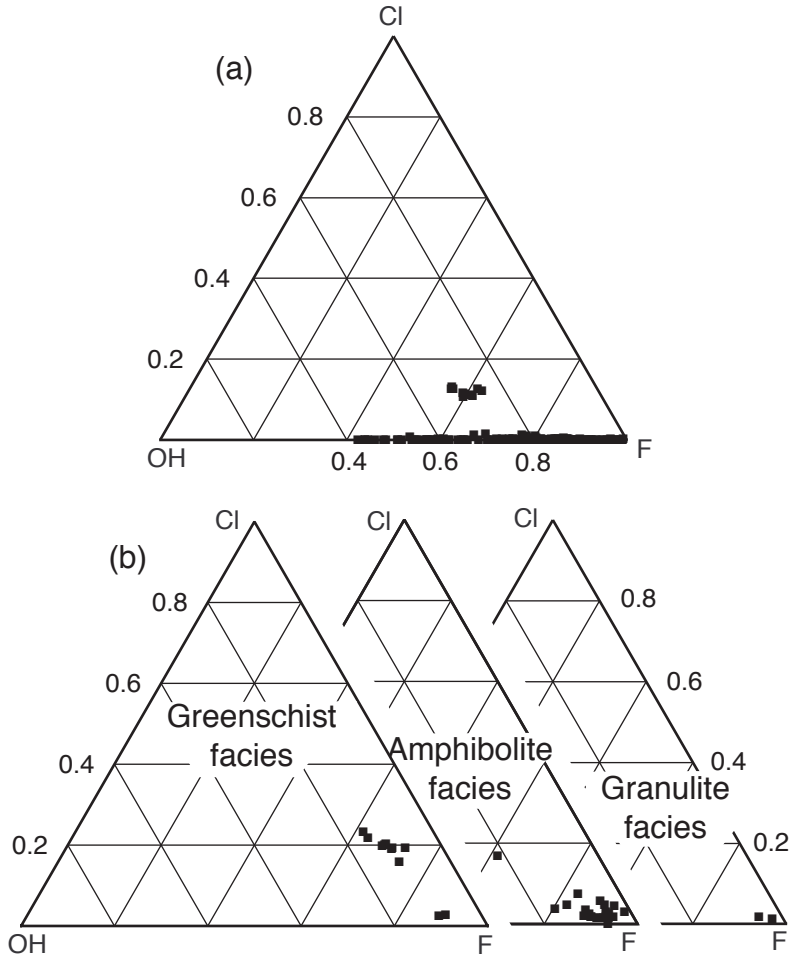
(a)
Cl
0.8
0.6
0.4
0.2
OH
0.4
0.6
0.8
F
(b)
Cl
Cl
Cl
0.8
0.6
0.4
0.2
Greenschist facies
Amphibolite facies
Granulite facies
OH
F
F
F

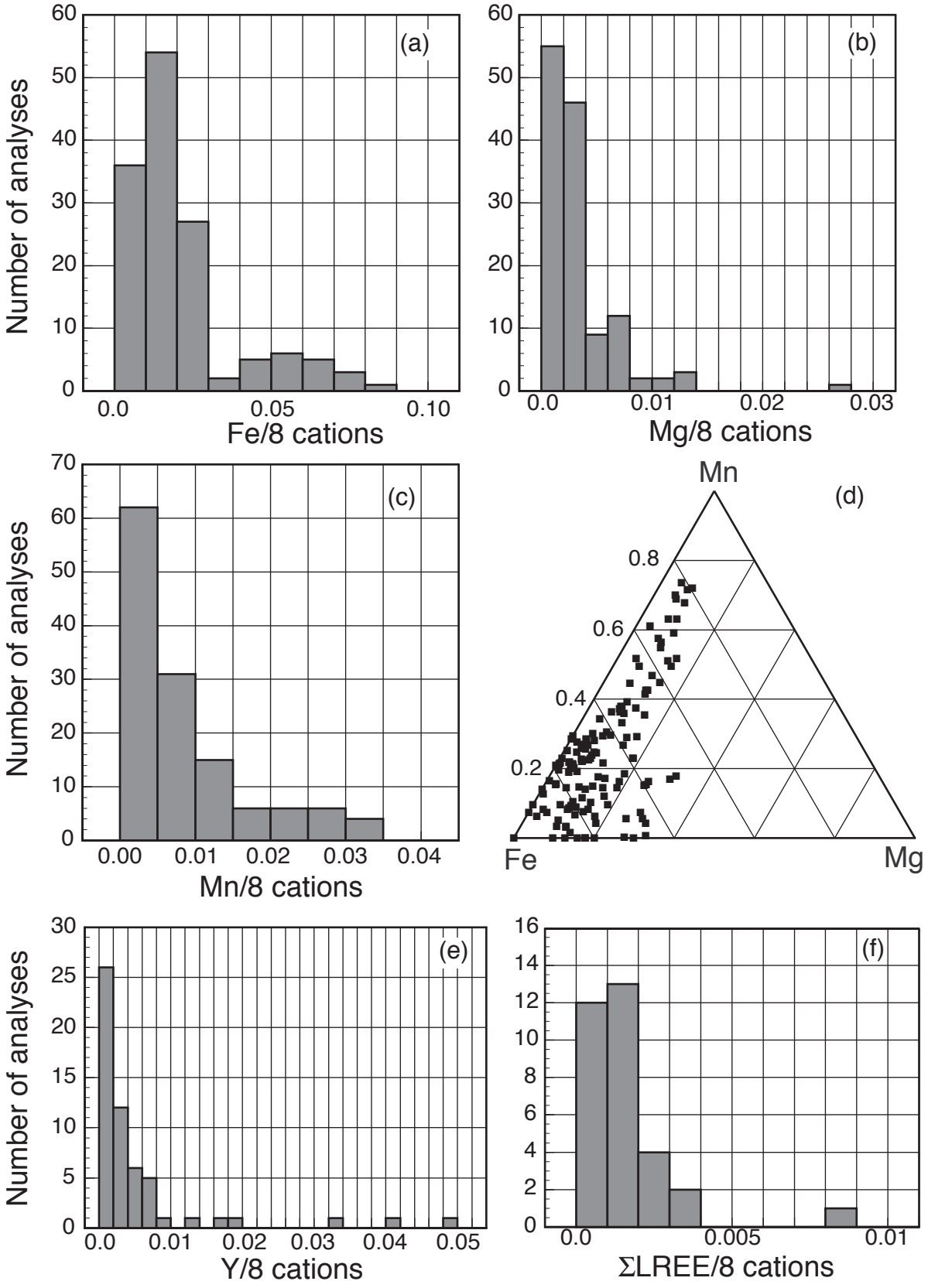
(a)
Number of analyses
Fe/8 cations
0.0
0.05
0.10
(b)
Mg/8 cations
0.0
0.01
0.02
0.03
(c)
Mn/8 cations
0.00
0.01
0.02
0.03
0.04
(d)
Mn
Fe
Mg
0.2
0.4
0.6
0.8
(e)
Y/8 cations
0.0
0.01
0.02
0.03
0.04
0.05
(f)
ΣLREE/8 cations
0.0
0.005
0.01

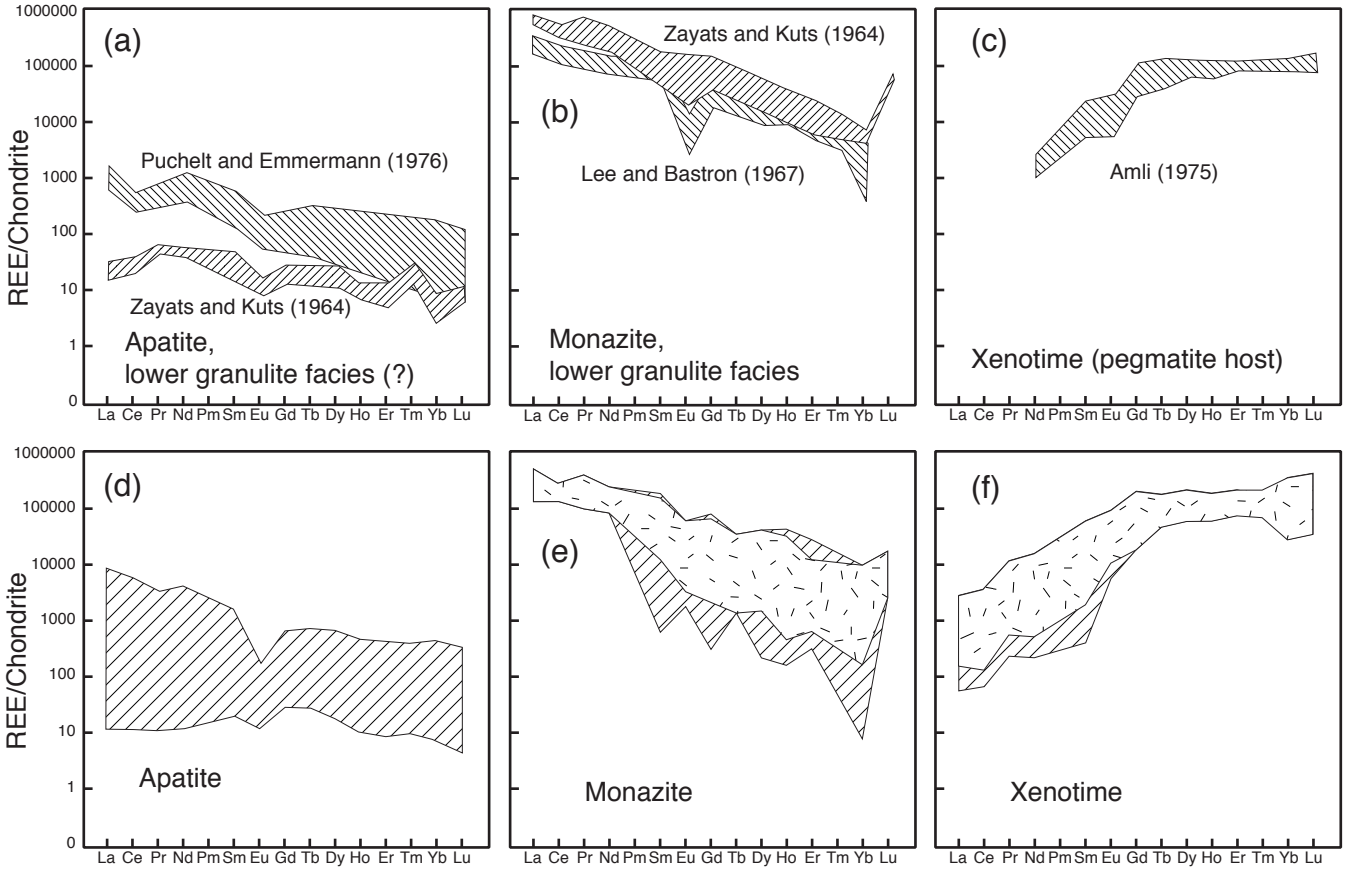
(a)
Puchelt and Emmermann (1976)
Zayats and Kuts (1964)
Apatite,
lower granulite facies (?)
(b)
Zayats and Kuts (1964)
Lee and Bastron (1967)
Monazite,
lower granulite facies
(c)
Amli (1975)
Xenotime (pegmatite host)
(d)
Apatite
(e)
Monazite
(f)
Xenotime
REE/Chondrite
1000000
100000
10000
1000
100
10
1
0
La Ce Pr Nd Pm Sm Eu Gd Tb Dy Ho Er Tm Yb Lu

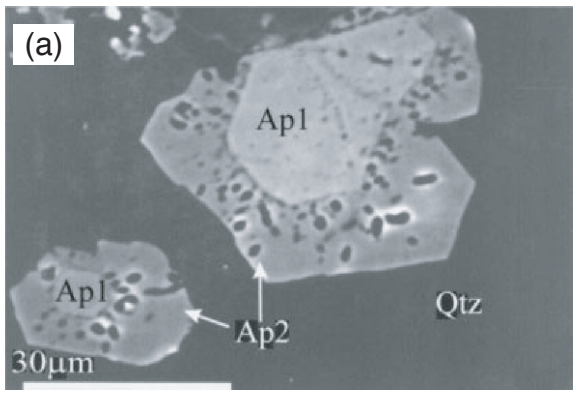
(a)
Ap1
Ap1
Ap2
Qtz
30µm

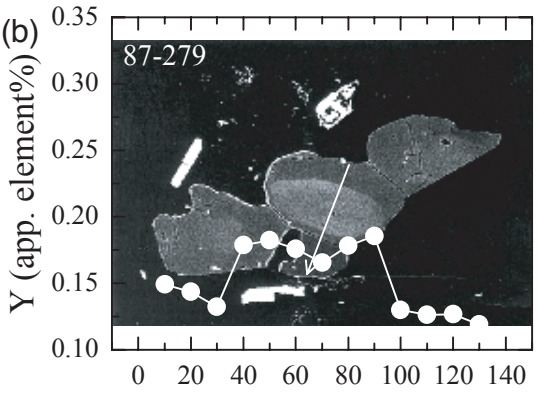
(b)
87-279
Y (app. element%)
0.35
0.30
0.25
0.20
0.15
0.10
0
20
40
60
80
100
120
140

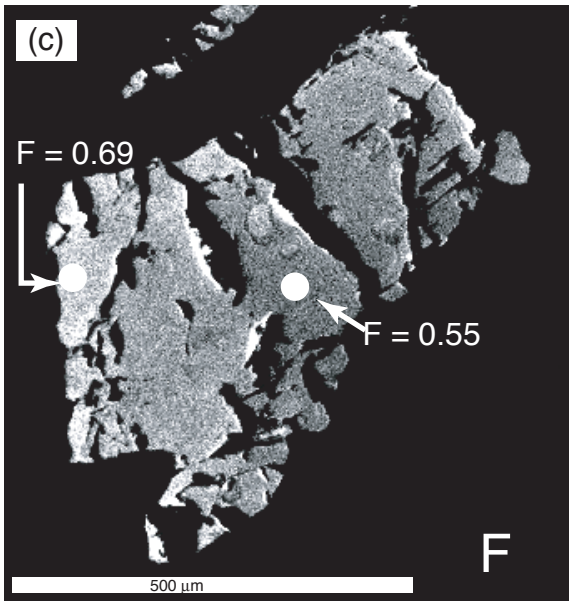
(c)
F = 0.69
F = 0.55
F
500 µm

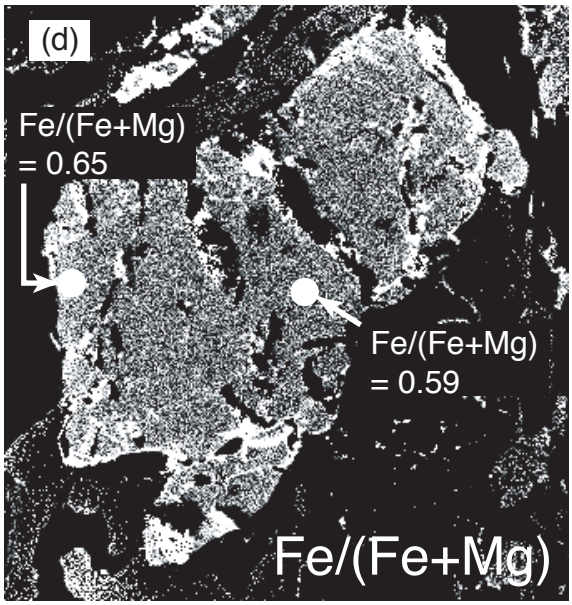
(d)
Fe/(Fe+Mg)
= 0.65
Fe/(Fe+Mg)
= 0.59
Fe/(Fe+Mg)

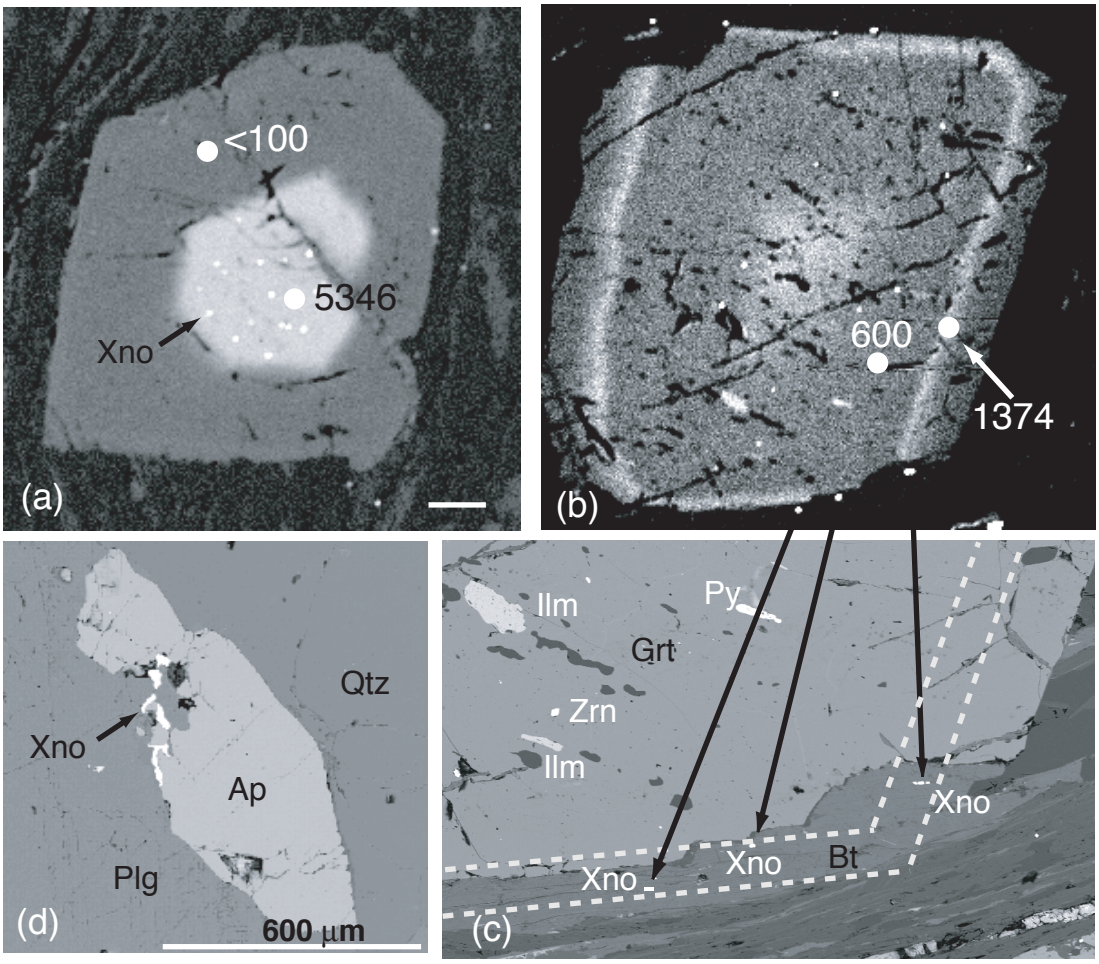
<100
5346
Xno
(a)
600
1374
(b)
Qtz
Xno
Ap
Plg
(d)
600 µm
Ilm
Py
Grt
Zrn
Ilm
Xno
Xno
Xno
Bt
(c)

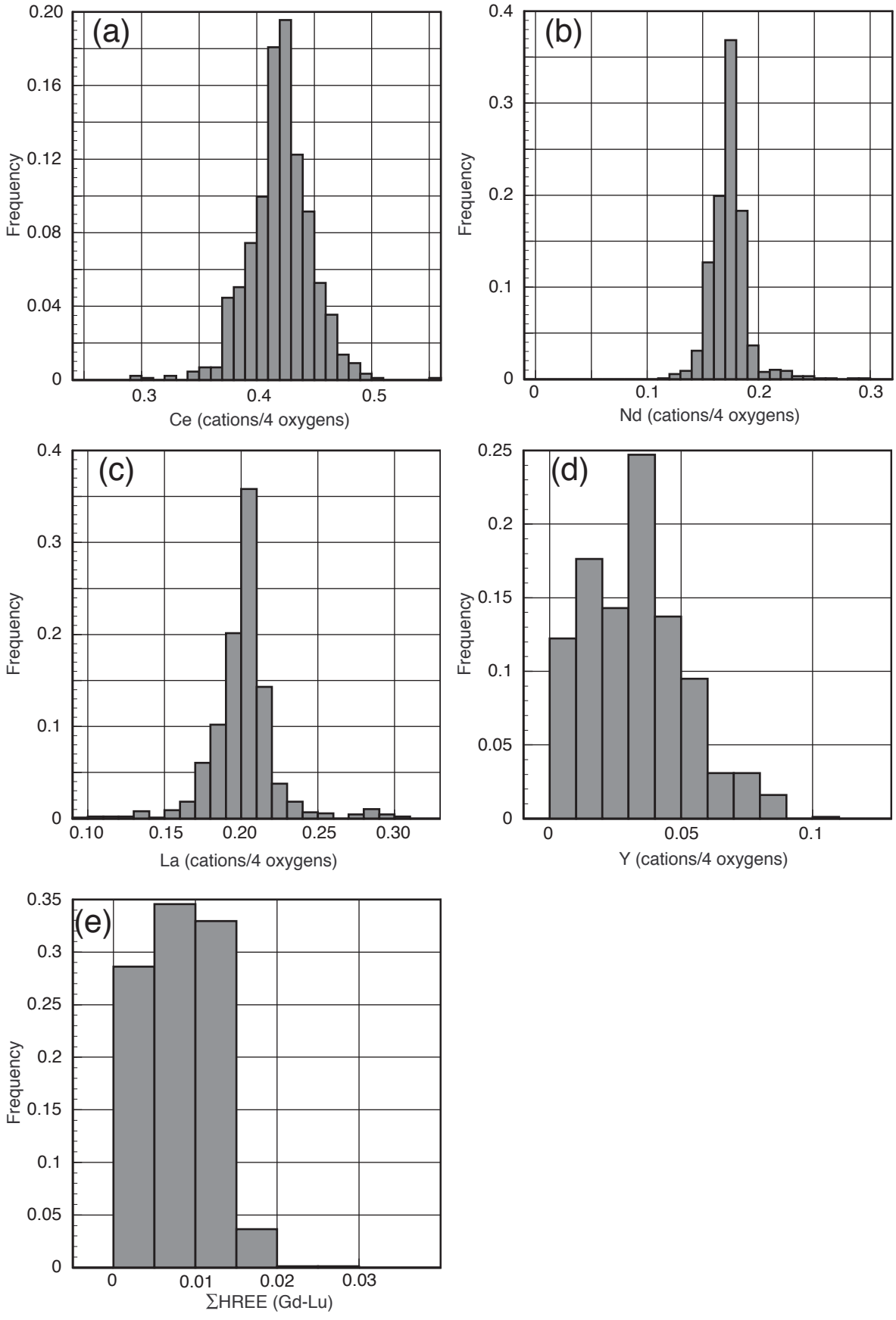
(a)
Frequency
0.20
0.16
0.12
0.08
0.04
0
0.3
0.4
0.5
Ce (cations/4 oxygens)
(b)
Frequency
0.4
0.3
0.2
0.1
0
0
0.1
0.2
0.3
Nd (cations/4 oxygens)
(c)
Frequency
0.4
0.3
0.2
0.1
0
0.10
0.15
0.20
0.25
0.30
La (cations/4 oxygens)
(d)
Frequency
0.25
0.2
0.15
0.1
0.05
0
0
0.05
0.1
Y (cations/4 oxygens)
(e)
Frequency
0.35
0.3
0.25
0.2
0.15
0.1
0.05
0
0
0.01
0.02
0.03
ΣHREE (Gd-Lu)

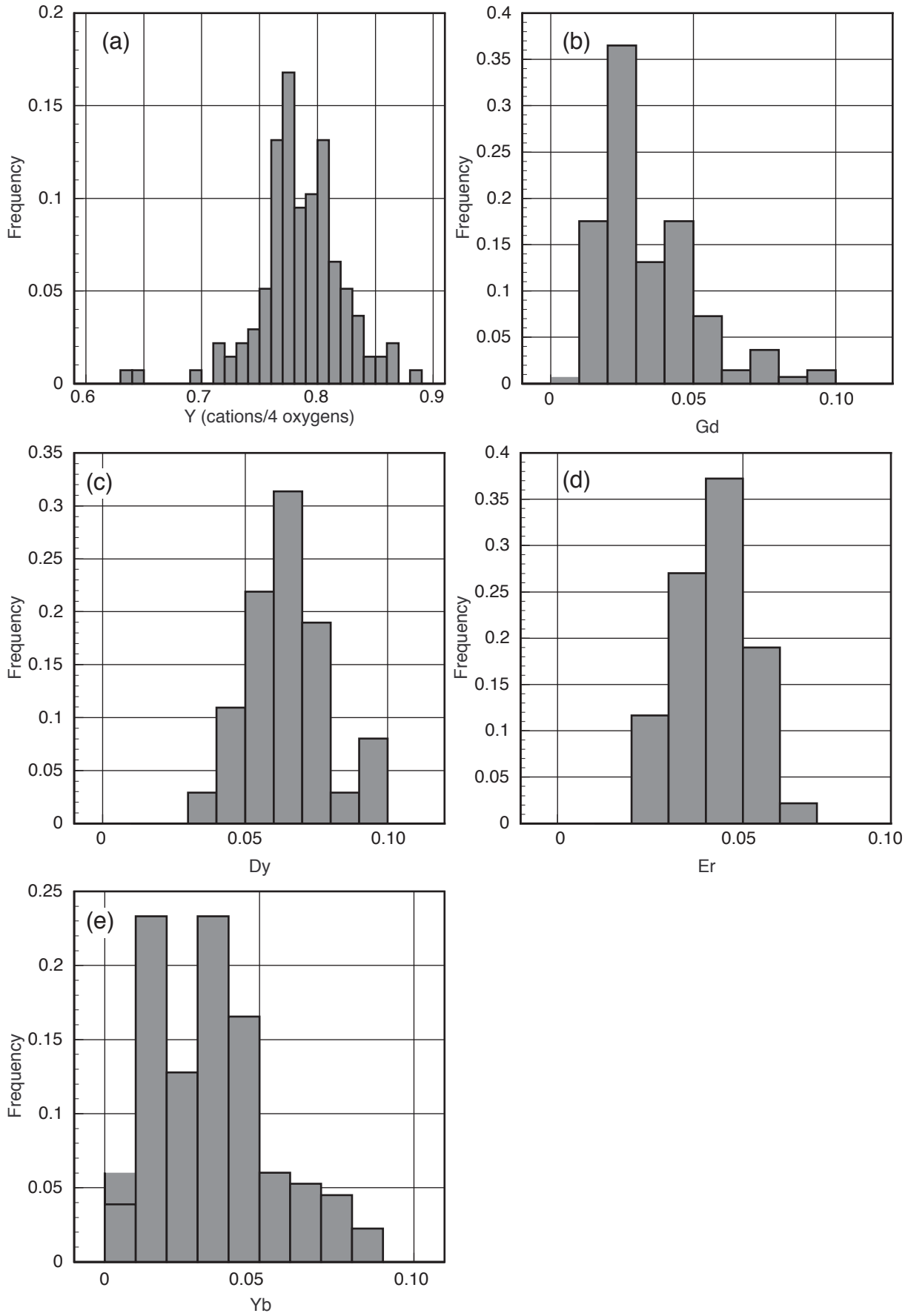
(a)
Frequency
0.2
0.15
0.1
0.05
0
0.6
0.7
0.8
0.9
Y (cations/4 oxygens)
(b)
Frequency
0.4
0.35
0.3
0.25
0.2
0.15
0.1
0.05
0
0
0.05
0.10
Gd
(c)
Frequency
0.35
0.3
0.25
0.2
0.15
0.1
0.05
0
0
0.05
0.10
Dy
(d)
Frequency
0.4
0.35
0.3
0.25
0.2
0.15
0.1
0.05
0
0
0.05
0.10
Er
(e)
Frequency
0.25
0.2
0.15
0.1
0.05
0
0
0.05
0.10
Yb

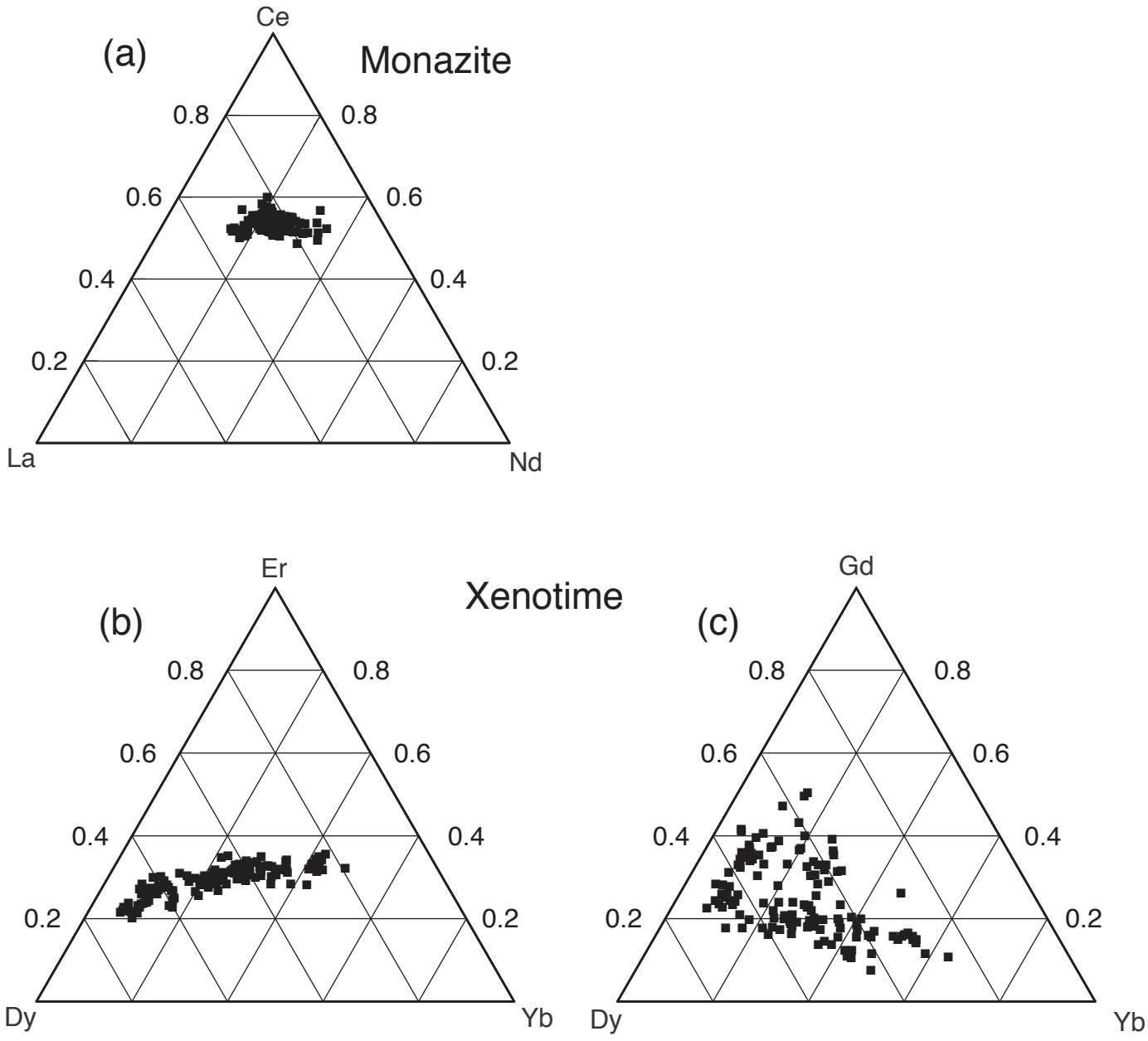
(a)
Monazite
Ce
La
Nd
0.8
0.6
0.4
0.2
(b)
Xenotime
Er
Dy
Yb
(c)
Gd
Dy
Yb

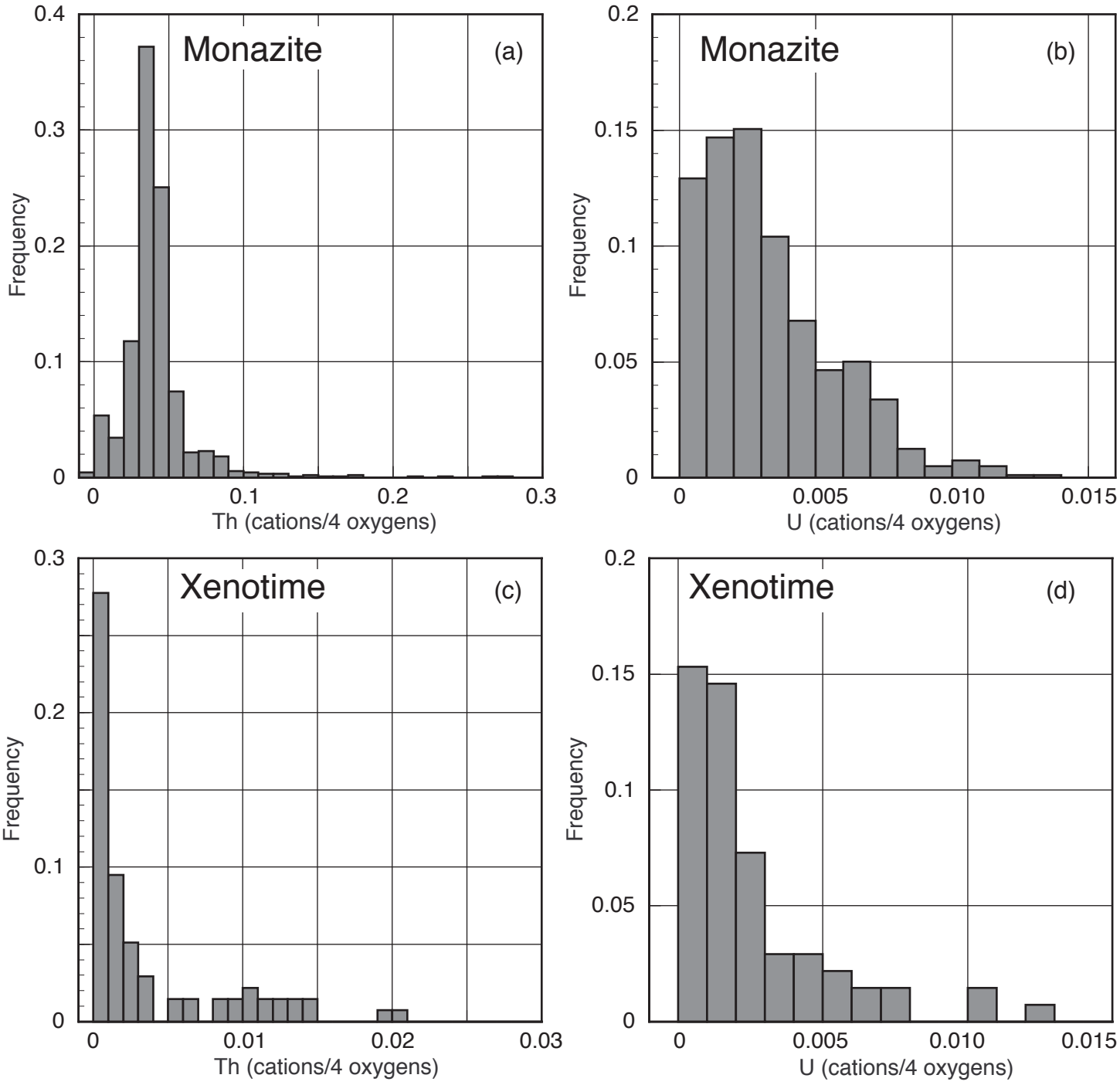
Monazite
(a)
Frequency
0.4
0.3
0.2
0.1
0
0
0.1
0.2
0.3
Th (cations/4 oxygens)
Monazite
(b)
Frequency
0.2
0.15
0.1
0.05
0
0
0.005
0.010
0.015
U (cations/4 oxygens)
Xenotime
(c)
Frequency
0.3
0.2
0.1
0
0
0.01
0.02
0.03
Th (cations/4 oxygens)
Xenotime
(d)
Frequency
0.2
0.15
0.1
0.05
0
0
0.005
0.010
0.015
U (cations/4 oxygens)

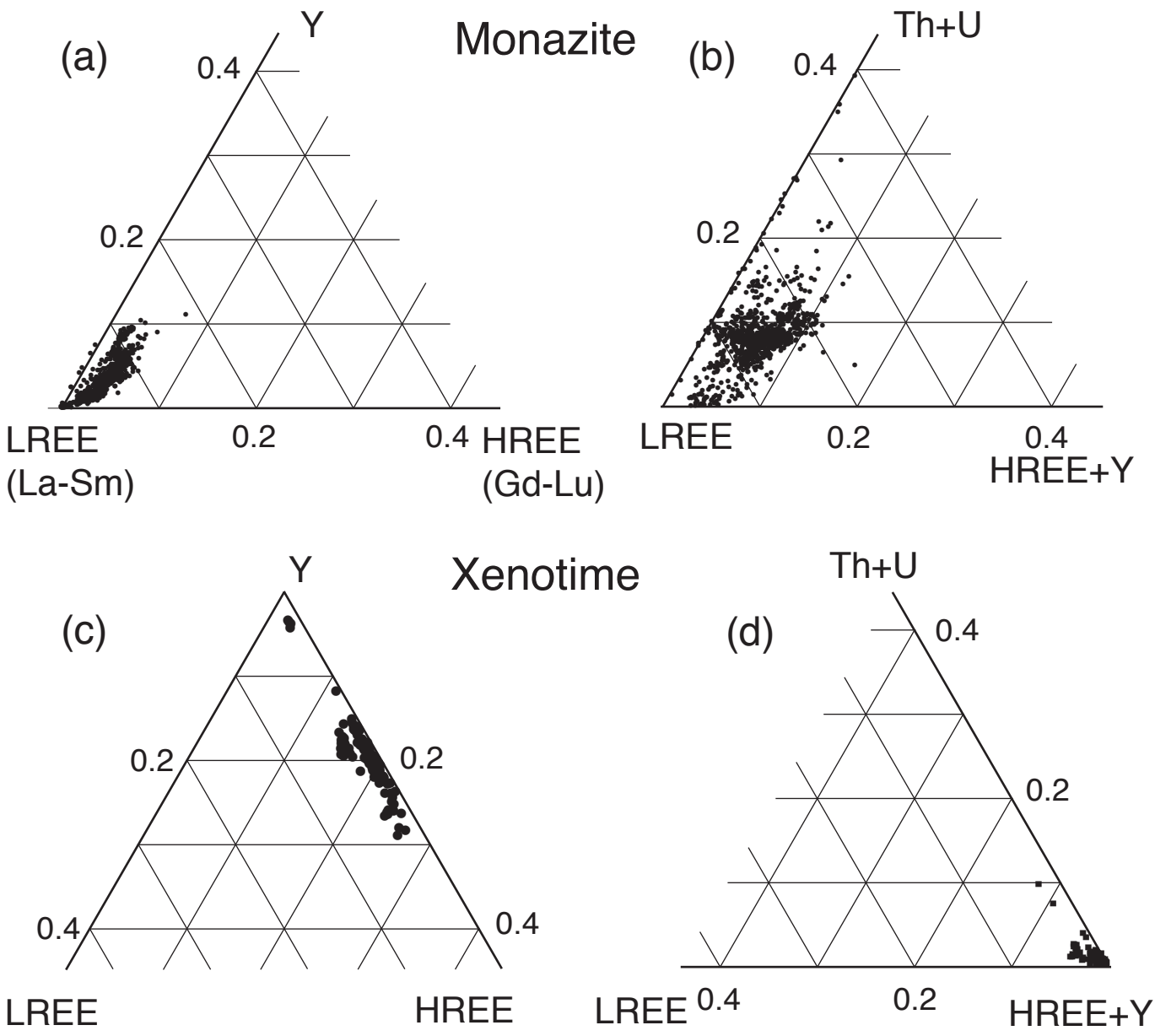
Monazite
(a)
Y
0.4
0.2
LREE
(La-Sm)
0.2
0.4
HREE
(Gd-Lu)
(b)
Th+U
0.4
0.2
LREE
0.2
0.4
HREE+Y
Xenotime
(c)
Y
0.2
0.2
0.4
0.4
LREE
HREE
(d)
Th+U
0.4
0.2
LREE
0.4
0.2
HREE+Y

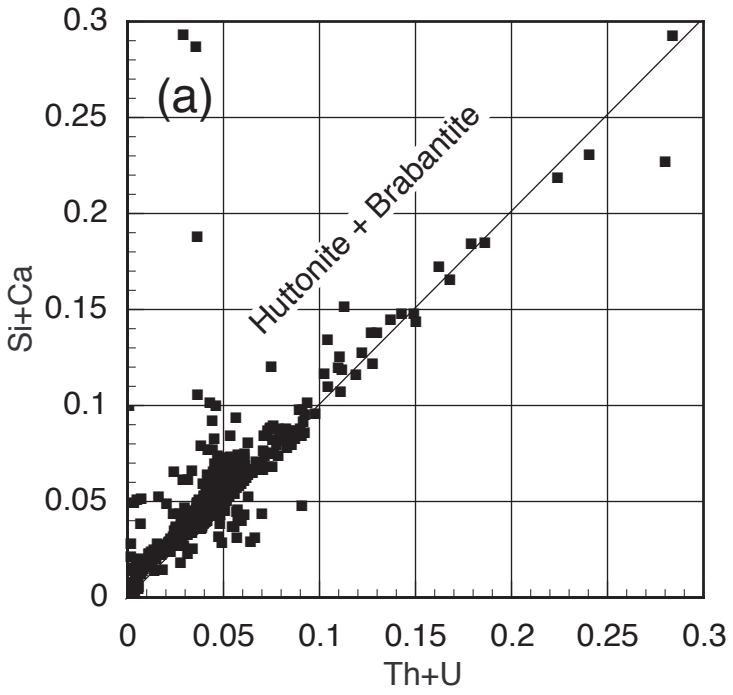
(a)
Huttonite + Brabantite
Si+Ca
Th+U
0
0.05
0.1
0.15
0.2
0.25
0.3

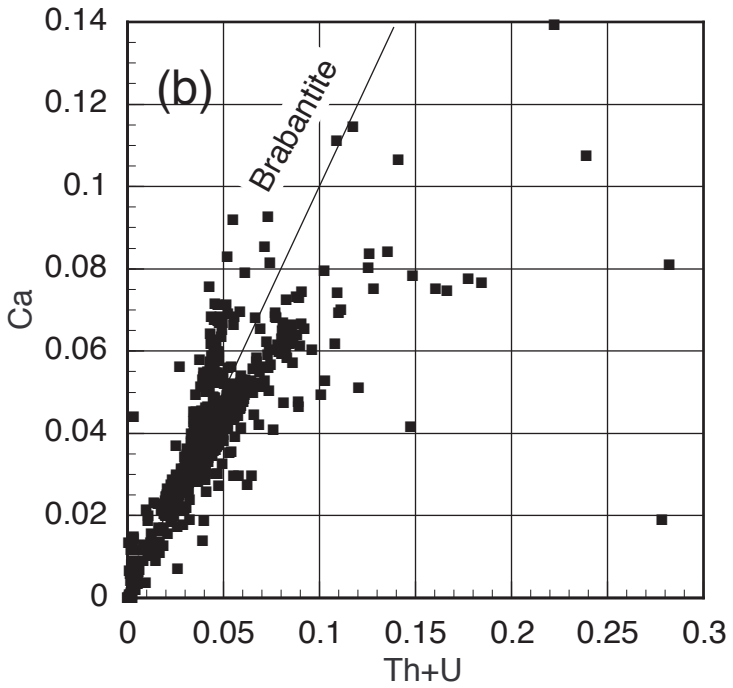
(b)
Brabantite
Ca
Th+U
0
0.02
0.04
0.06
0.08
0.1
0.12
0.14
0.05
0.15
0.2
0.25
0.3

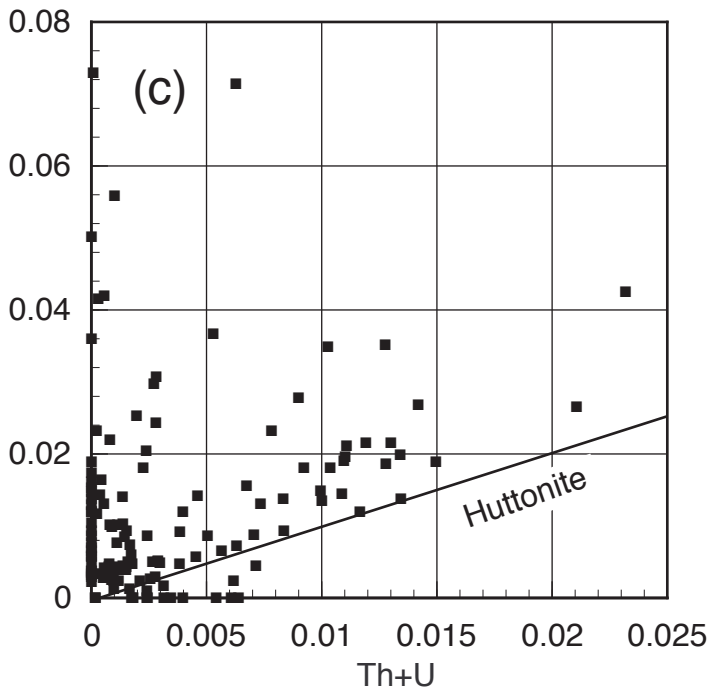
(c)
Huttonite
Si
Th+U
0
0.02
0.04
0.06
0.08
0.005
0.01
0.015
0.02
0.025

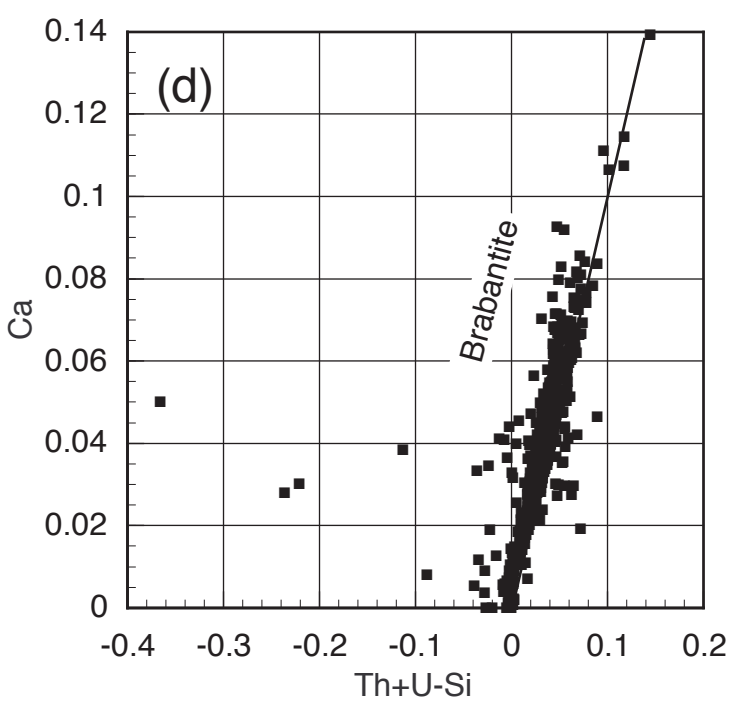
(d)
Brabantite
Ca
Th+U-Si
0
0.02
0.04
0.06
0.08
0.1
0.12
0.14
-0.4
-0.3
-0.2
-0.1
0
0.1
0.2

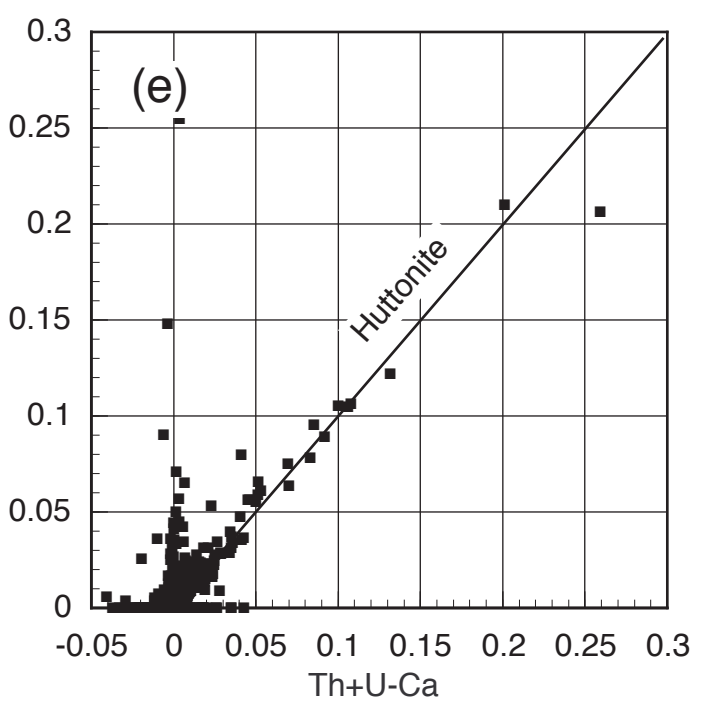
(e)
Huttonite
Si
Th+U-Ca
0
0.05
0.1
0.15
0.2
0.25
0.3
-0.05
0
0.05
0.1
0.15
0.2
0.25
0.3

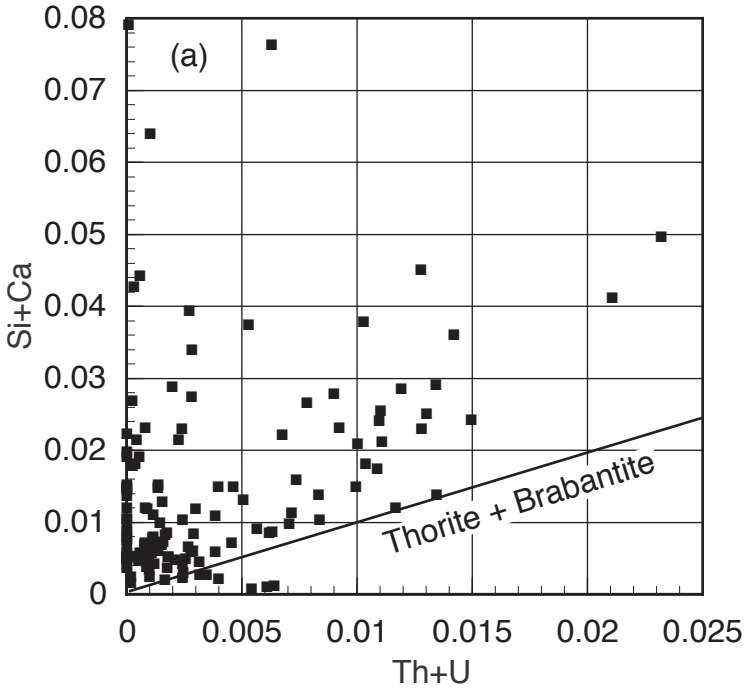
(a)
Si+Ca
Th+U
Thorite + Brabantite
0.08
0.07
0.06
0.05
0.04
0.03
0.02
0.01
0
0.005
0.01
0.015
0.02
0.025

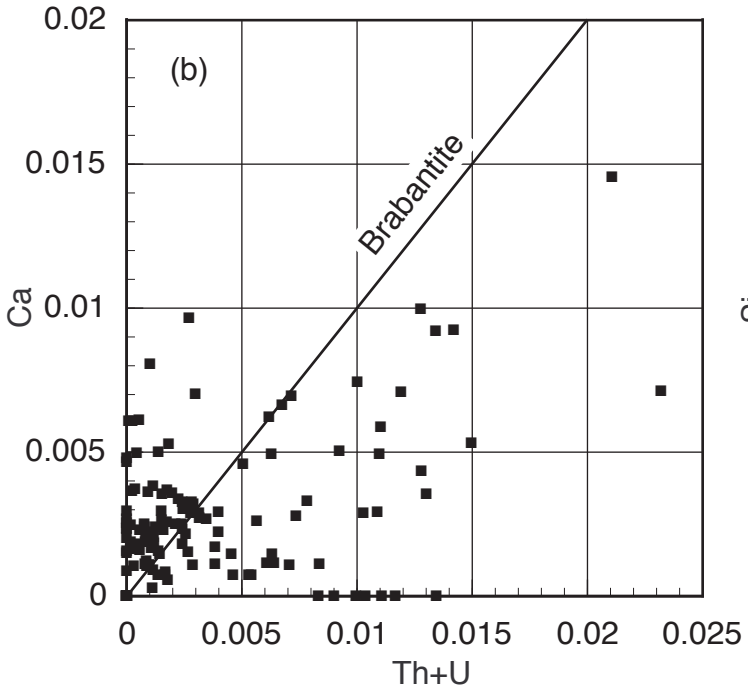
(b)
Ca
Th+U
Brabantite
0.02
0.015
0.01
0.005
0
0.005
0.01
0.015
0.02
0.025

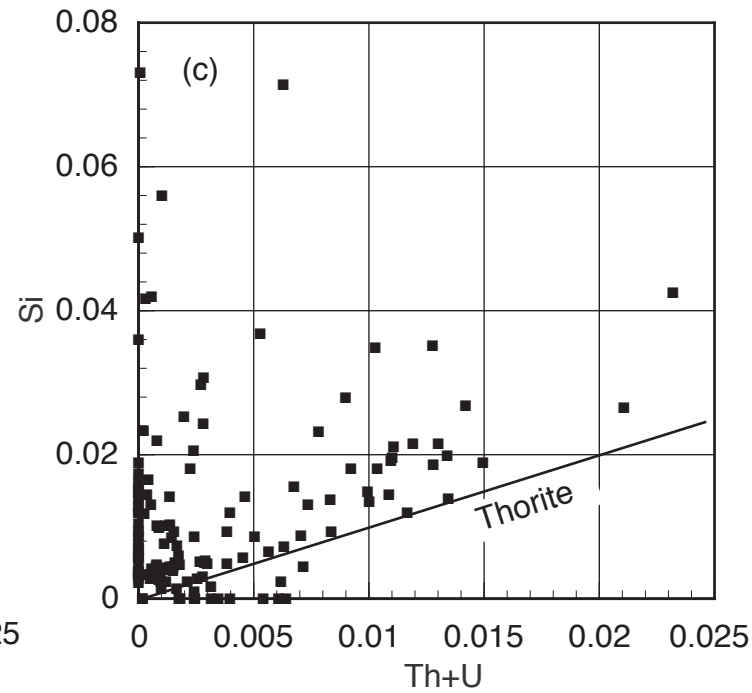
(c)
Si
Th+U
Thorite
0.08
0.06
0.04
0.02
0
0.005
0.01
0.015
0.02
0.025

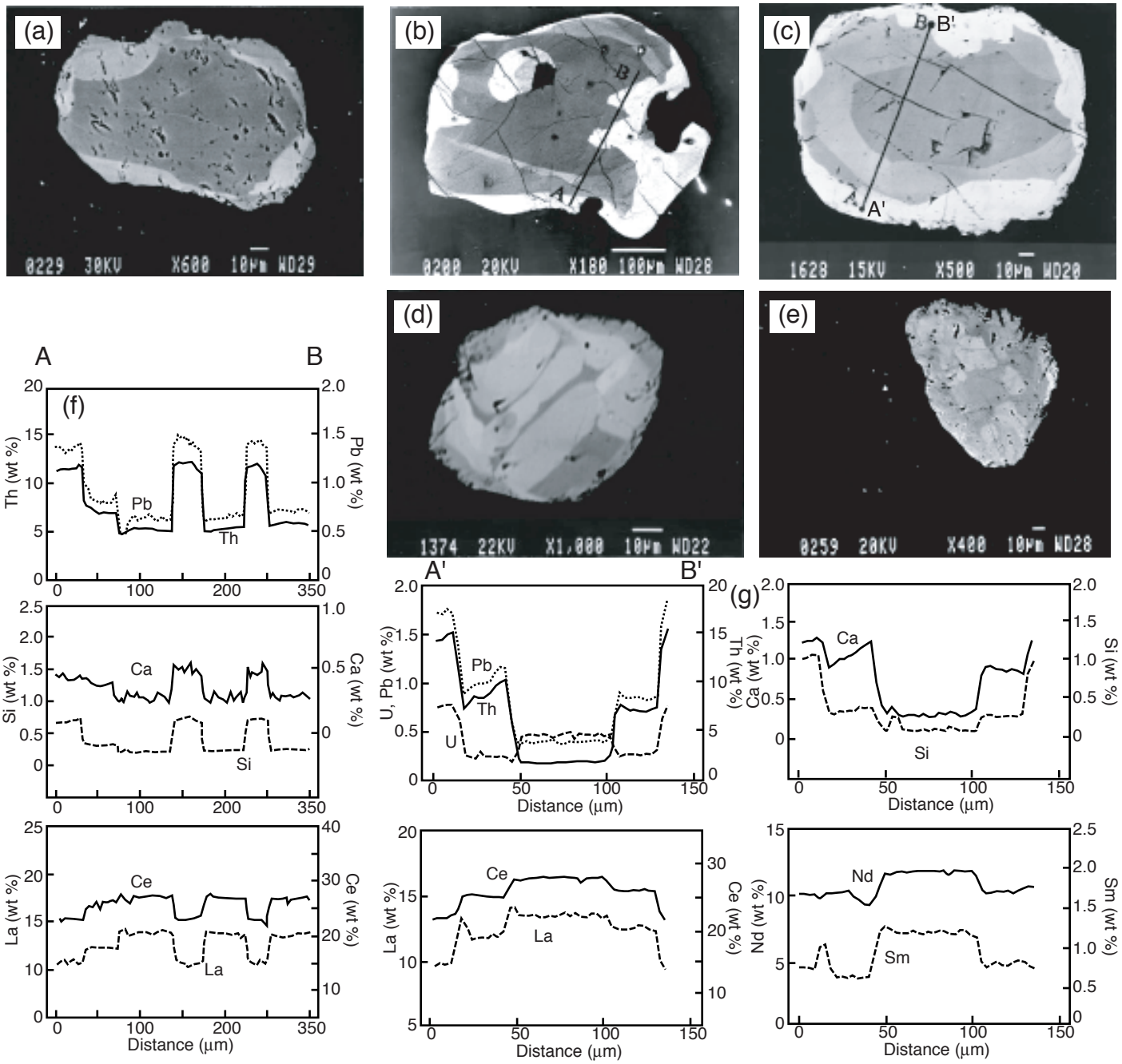
(a)
0229 30KV X600 10µm WD29
(b)
0200 20KV X180 100µm WD28
(c)
B
B'
A
A'
1628 15KV X500 10µm WD20
(d)
1374 22KV X1,000 10µm WD22
(e)
0259 20KV X400 10µm WD28
A
B
(f)
Th (wt %)
Pb (wt %)
Pb
Th
Si (wt %)
Ca (wt %)
Ca
Si
La (wt %)
Ce (wt %)
Ce
La
Distance (µm)
A'
B'
U, Pb (wt %)
Th (wt %)
Pb
Th
U
Distance (µm)
(g)
Ca (wt %)
Si (wt %)
Ca
Si
Distance (µm)
La (wt %)
Ce (wt %)
Ce
La
Distance (µm)
Nd (wt %)
Sm (wt %)
Nd
Sm
Distance (µm)

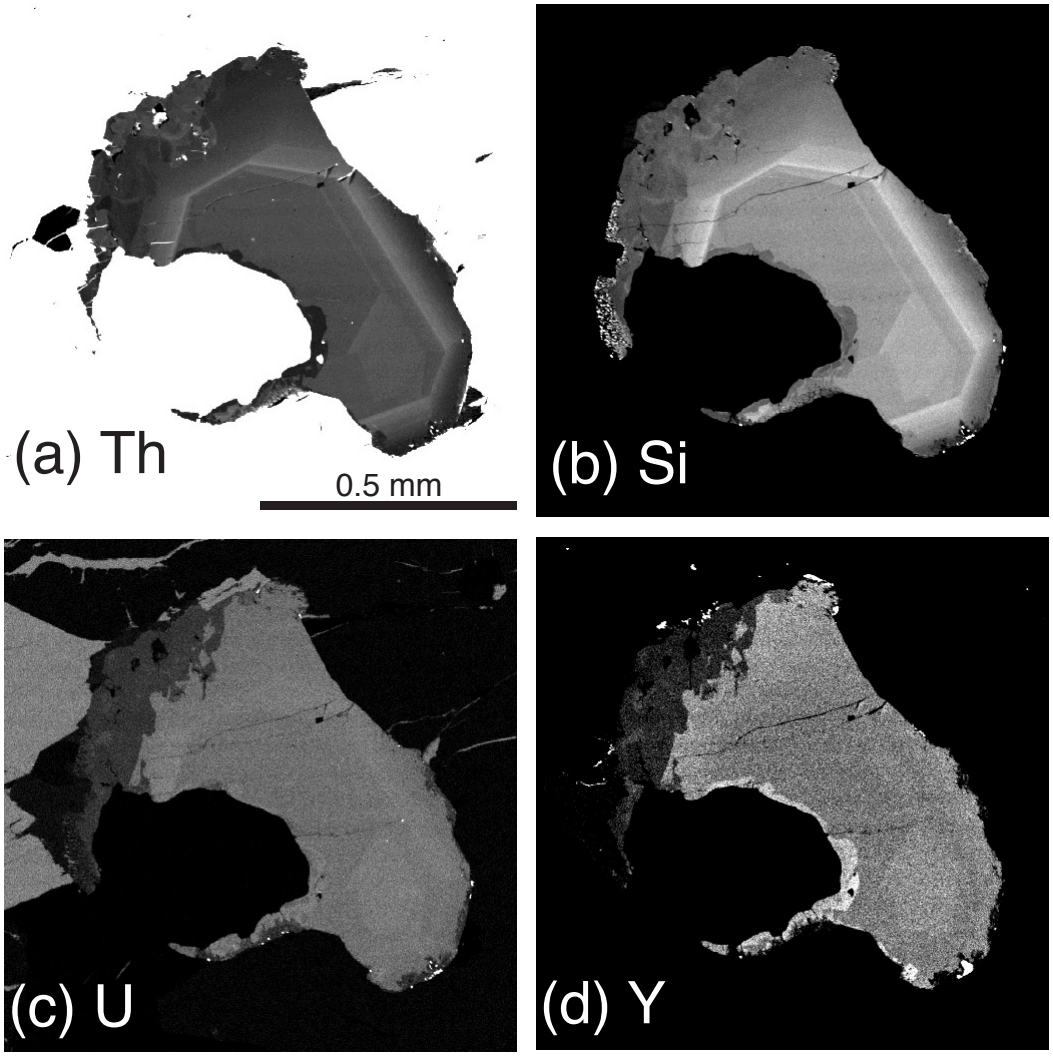
(a) Th
0.5 mm
(b) Si
(c) U
(d) Y

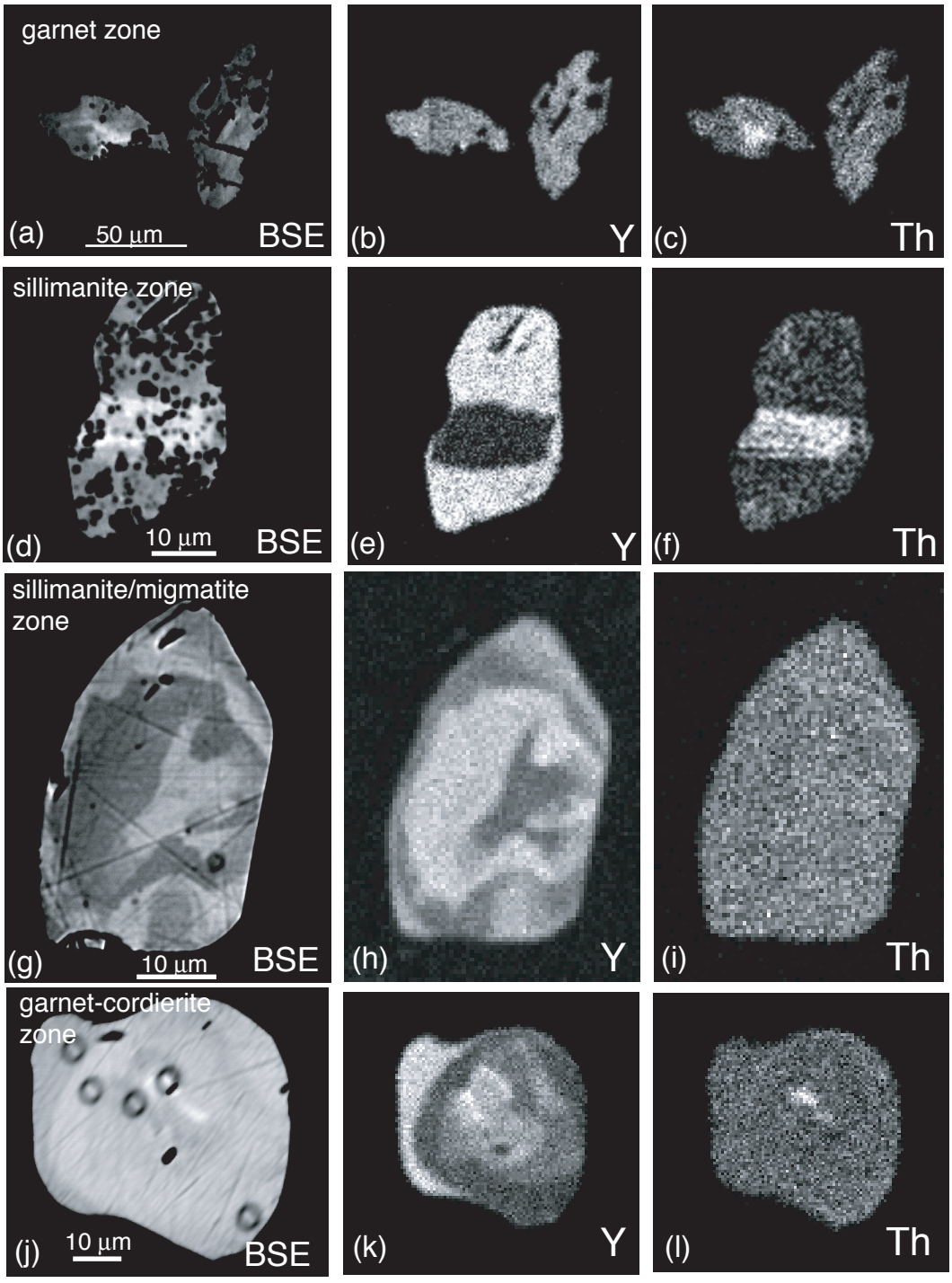
garnet zone
(a)
50 μm
BSE
(b)
Y
(c)
Th
sillimanite zone
(d)
10 μm
BSE
(e)
Y
(f)
Th
sillimanite/migmatite zone
(g)
10 μm
BSE
(h)
Y
(i)
Th
garnet-cordierite zone
(j)
10 μm
BSE
(k)
Y
(l)
Th

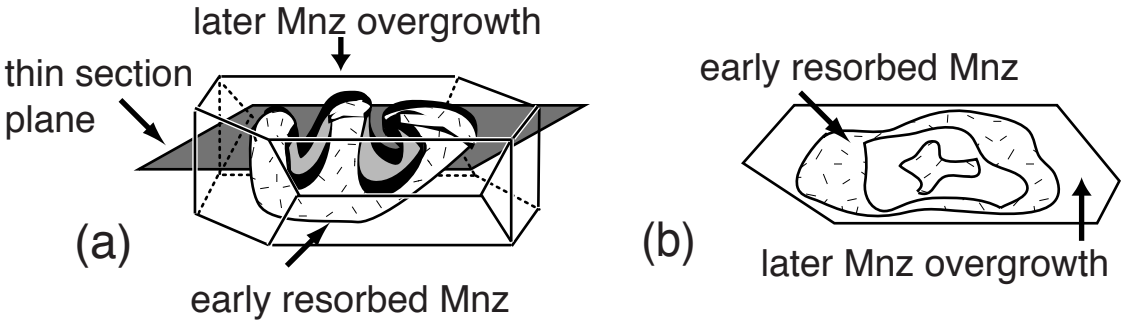
later Mnz overgrowth
thin section
plane
(a)
early resorbed Mnz
early resorbed Mnz
(b)
later Mnz overgrowth

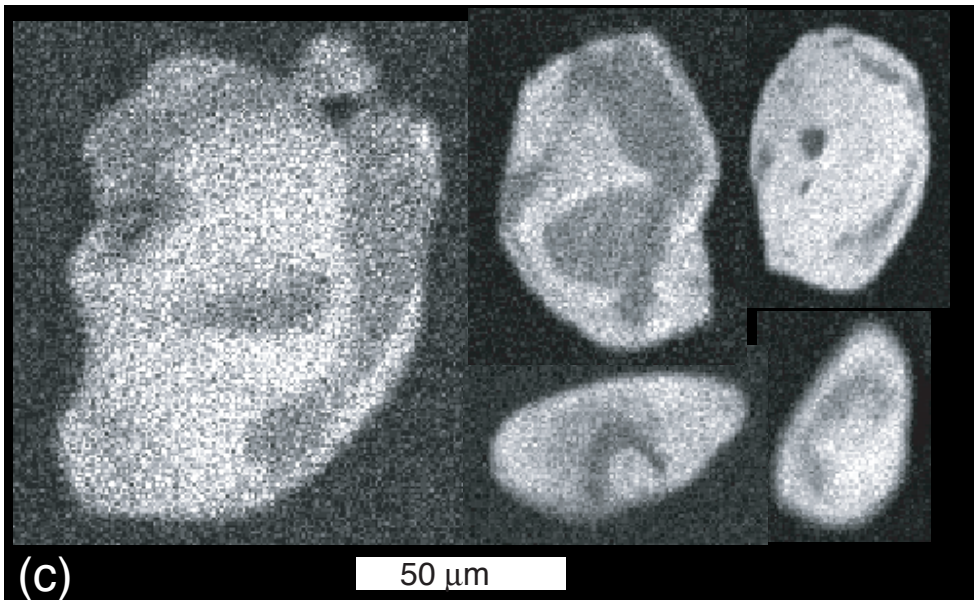
(c)
50 μm

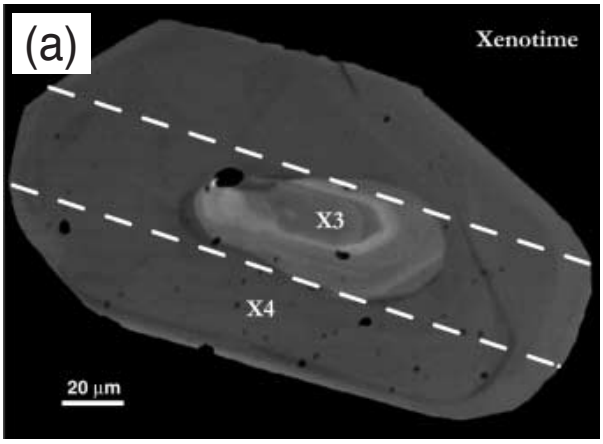
(a)
Xenotime
X3
X4
20 μm

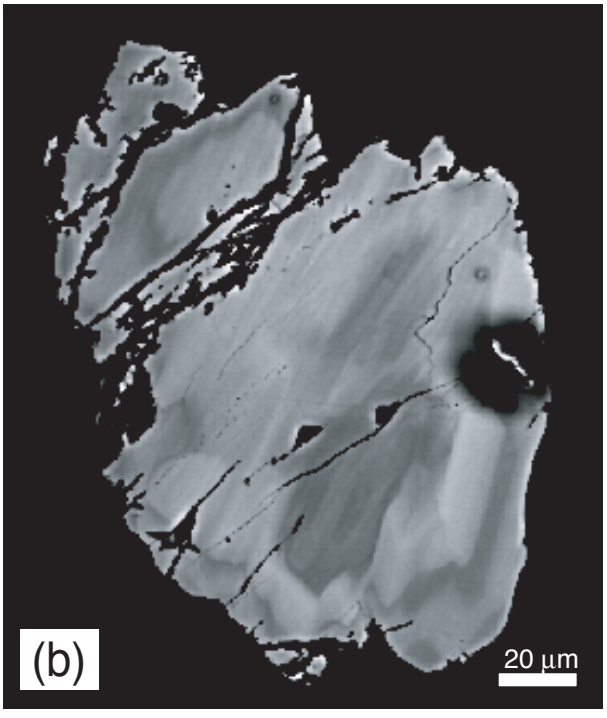
(b)
20 μm

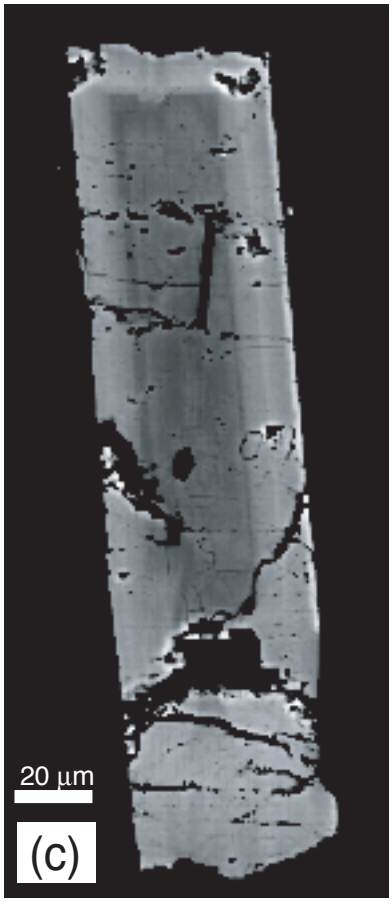
20 μm
(c)

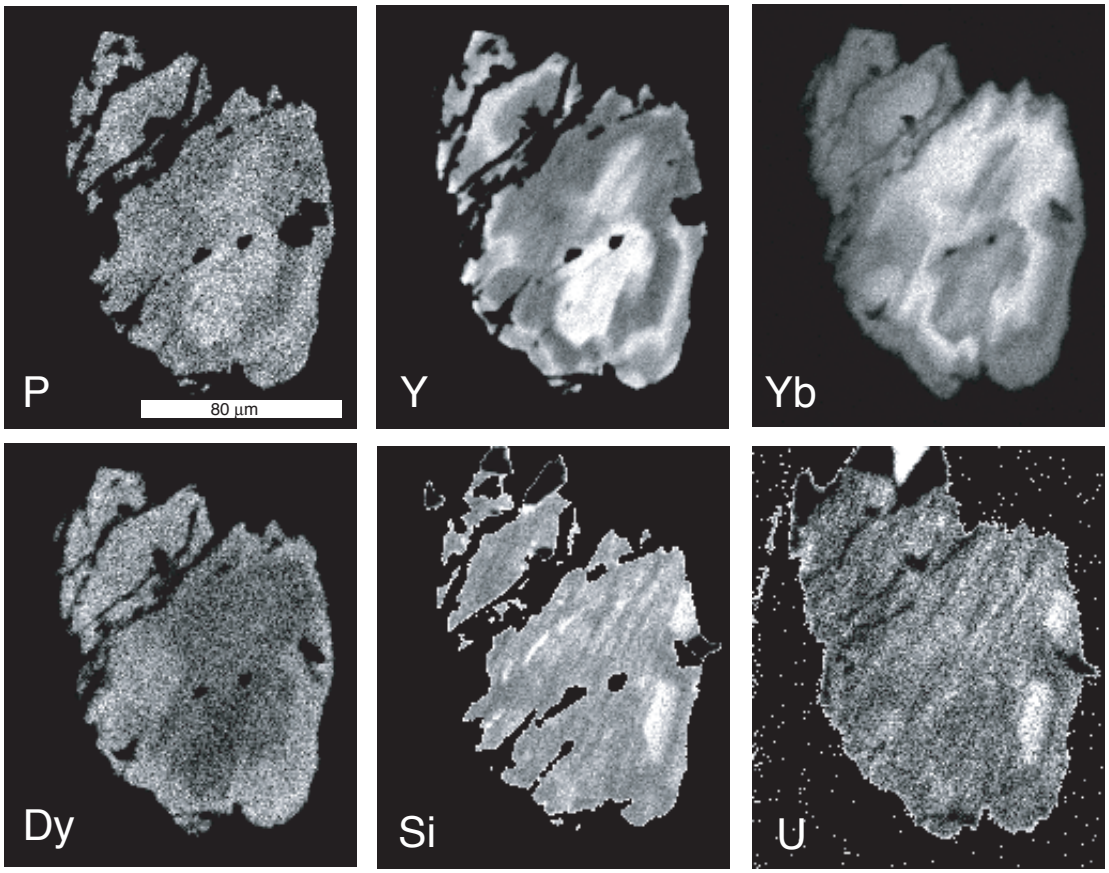
P
80 µm
Y
Yb
Dy
Si
U

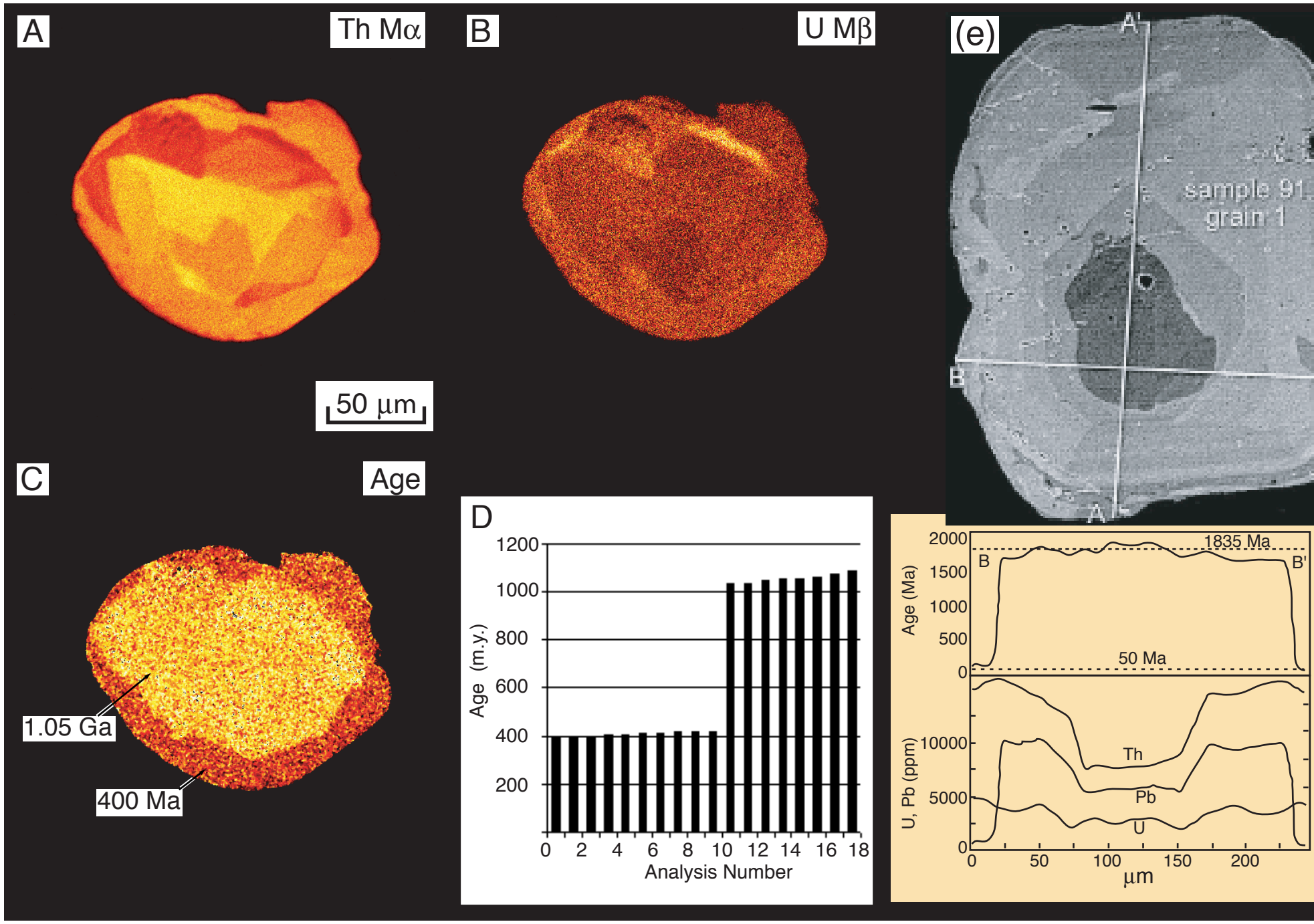
A
Th Mα
B
U Mβ
50 μm
C
Age
1.05 Ga
400 Ma
D
Age (m.y.)
1200
1000
800
600
400
200
0 2 4 6 8 10 12 14 16 18
Analysis Number
(e)
A'
B
A
sample 91
grain 1
2000
1500
1000
500
0
Age (Ma)
1835 Ma
B
B'
50 Ma
10000
5000
0
U, Pb (ppm)
Th
Pb
U
0 50 100 150 200
μm

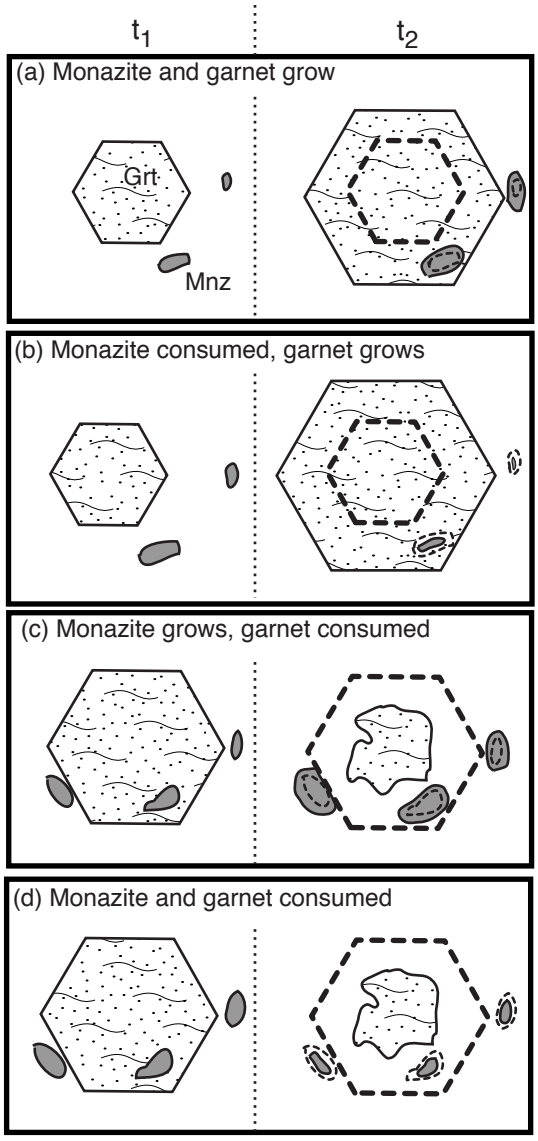
t1
t2
(a) Monazite and garnet grow
Grt
Mnz
(b) Monazite consumed, garnet grows
(c) Monazite grows, garnet consumed
(d) Monazite and garnet consumed

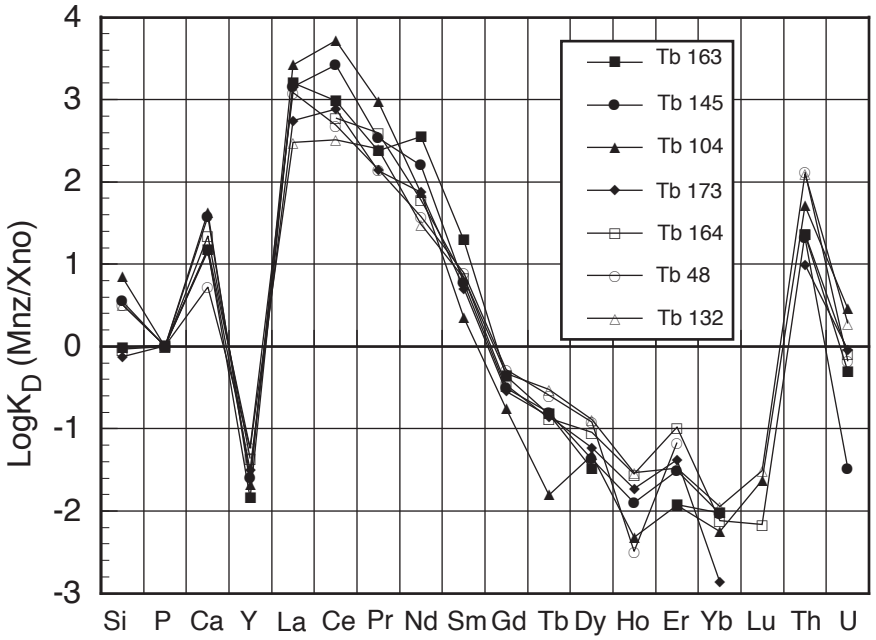
4
3
2
1
0
-1
-2
-3
LogK$_D$ (Mnz/Xno)
Si P Ca Y La Ce Pr Nd Sm Gd Tb Dy Ho Er Yb Lu Th U
Tb 163
Tb 145
Tb 104
Tb 173
Tb 164
Tb 48
Tb 132

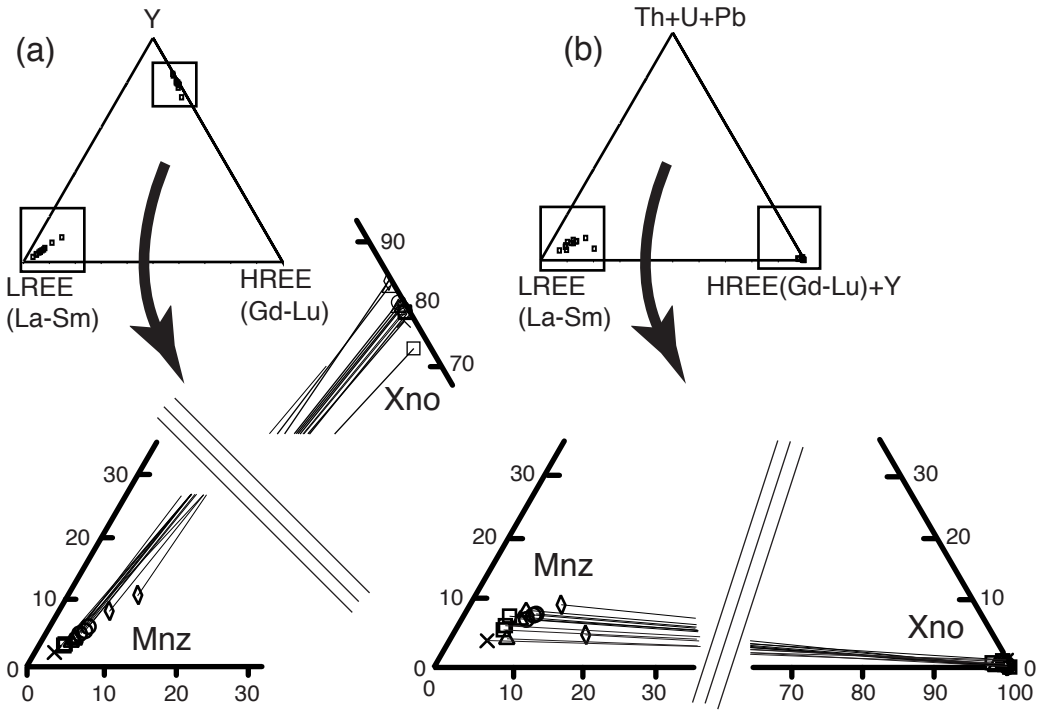
(a)
Y
LREE
(La-Sm)
HREE
(Gd-Lu)
90
80
70
Xno
30
20
10
0
Mnz
0
10
20
30
(b)
Th+U+Pb
LREE
(La-Sm)
HREE(Gd-Lu)+Y
Mnz
Xno
70
80
90
100

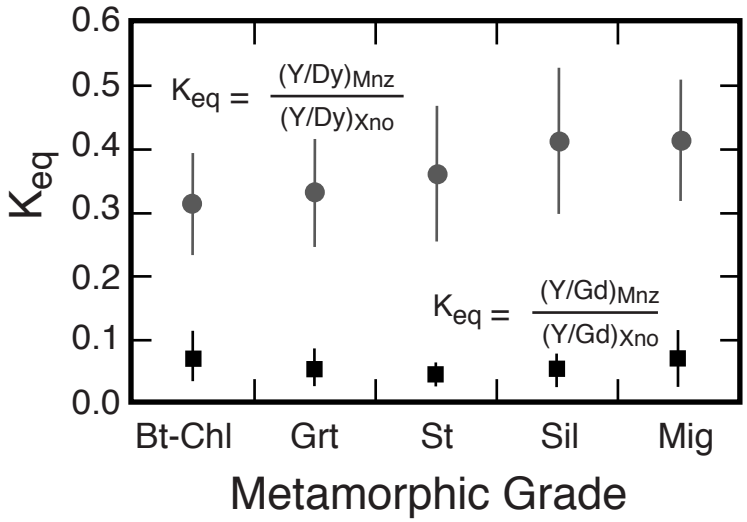
0.6
0.5
0.4
0.3
0.2
0.1
0.0
K_{eq}
$K_{eq} = \frac{(Y/Dy)_{Mnz}}{(Y/Dy)_{Xno}}$
$K_{eq} = \frac{(Y/Gd)_{Mnz}}{(Y/Gd)_{Xno}}$
Bt-Chl
Grt
St
Sil
Mig
Metamorphic Grade

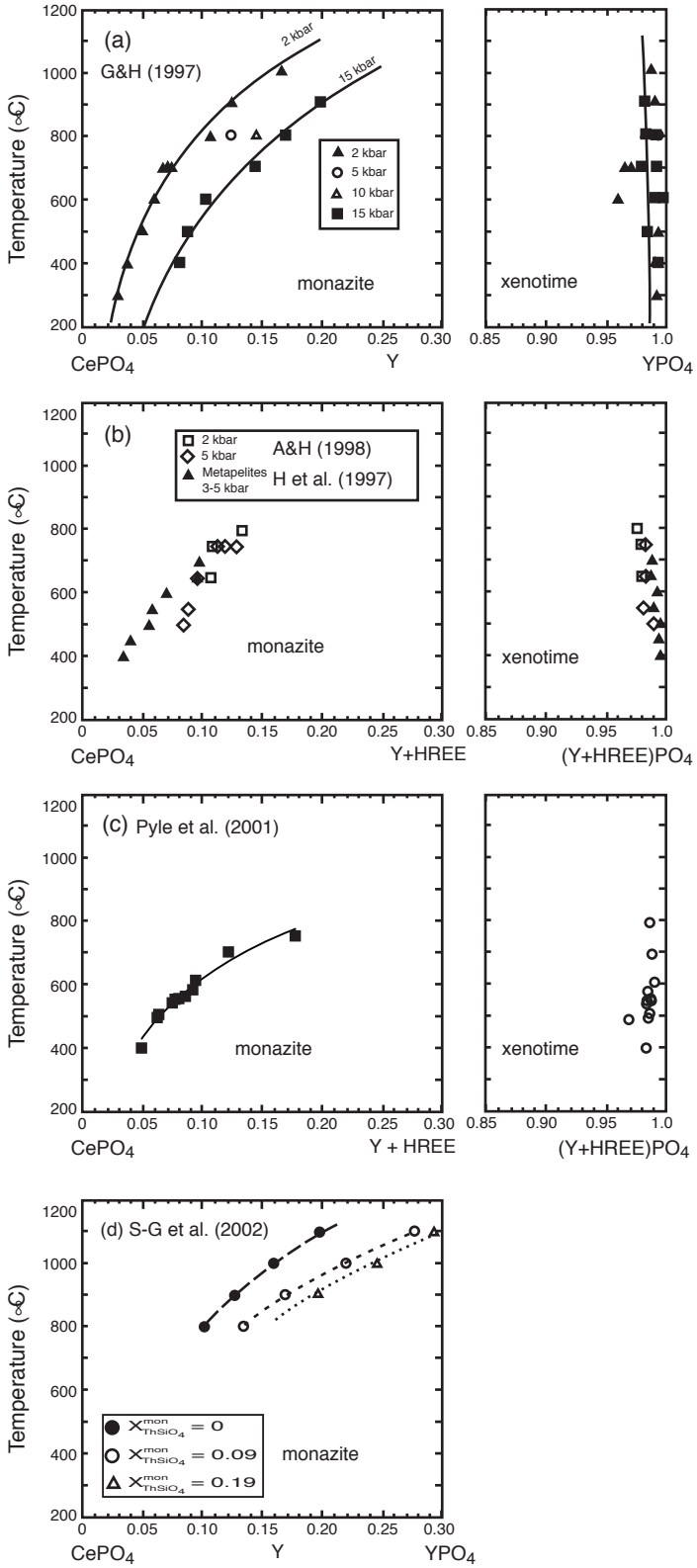
(a)
G&H (1997)
2 kbar
15 kbar
2 kbar
5 kbar
10 kbar
15 kbar
monazite
xenotime
Temperature (°C)
CePO4
Y
YPO4
(b)
2 kbar
5 kbar
Metapelites
3-5 kbar
A&H (1998)
H et al. (1997)
monazite
xenotime
Y+HREE
(Y+HREE)PO4
(c) Pyle et al. (2001)
monazite
xenotime
Y + HREE
(Y+HREE)PO4
(d) S-G et al. (2002)
monazite
Y

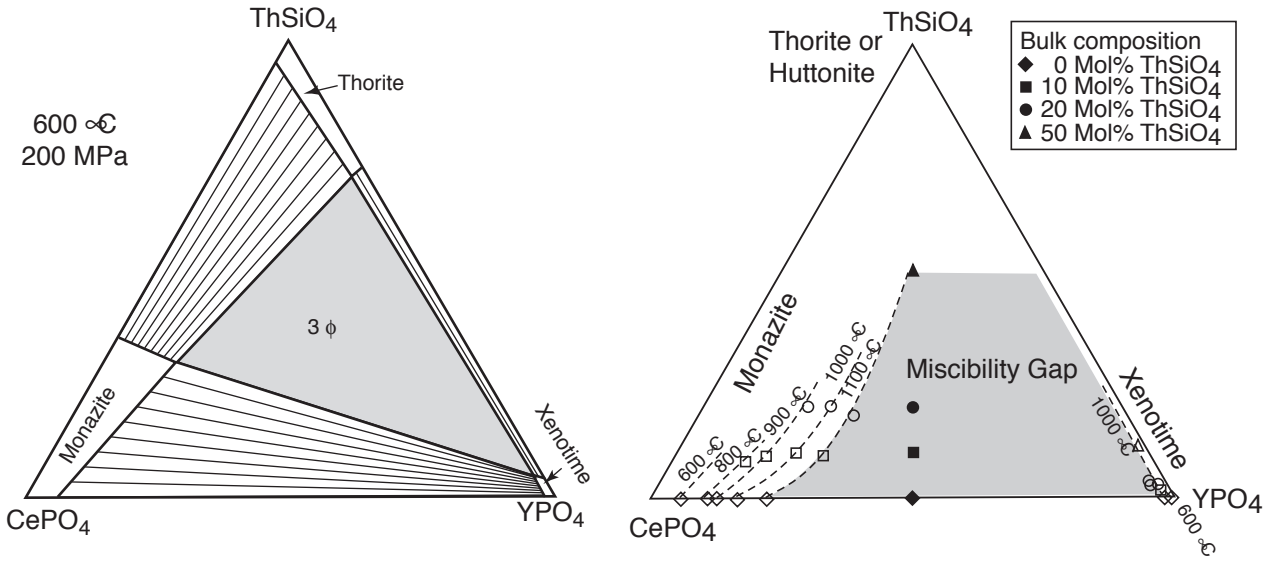
ThSiO4
Thorite
600 °C
200 MPa
3 ϕ
Monazite
Xenotime
CePO4
YPO4
ThSiO4
Thorite or
Huttonite
Bulk composition
0 Mol% ThSiO4
10 Mol% ThSiO4
20 Mol% ThSiO4
50 Mol% ThSiO4
Monazite
Miscibility Gap
Xenotime
600 °C
800 °C
900 °C
1000 °C
1100 °C
1000 °C
600 °C
CePO4
YPO4

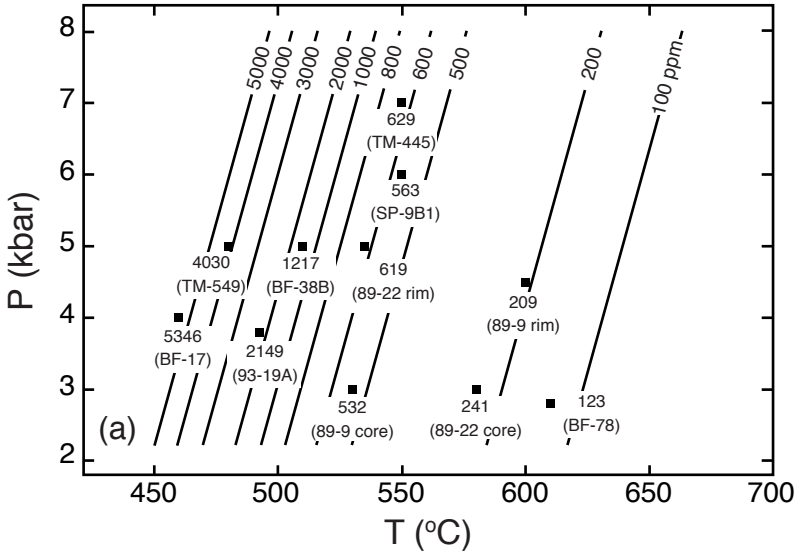
P (kbar)
T (°C)
5000
4000
3000
2000
1000
800
600
500
200
100 ppm
629
(TM-445)
563
(SP-9B1)
4030
(TM-549)
1217
(BF-38B)
619
(89-22 rim)
209
(89-9 rim)
5346
(BF-17)
2149
(93-19A)
532
(89-9 core)
241
(89-22 core)
123
(BF-78)
(a)

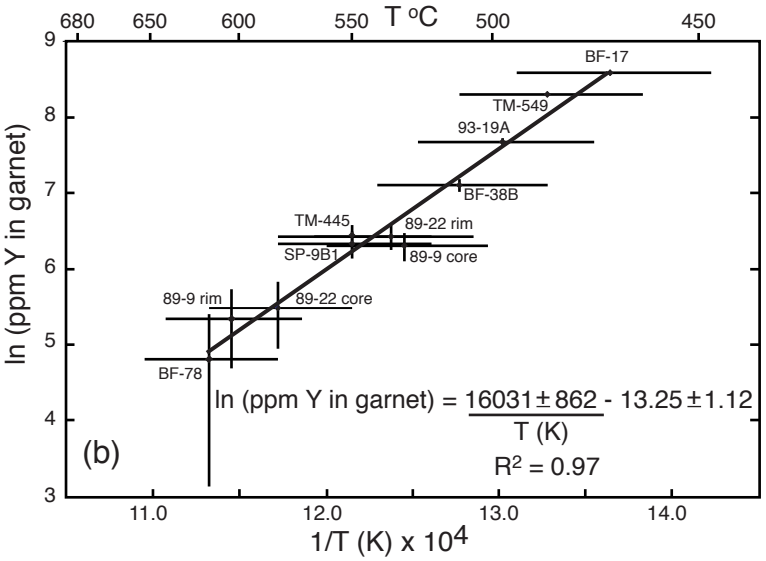
T °C
ln (ppm Y in garnet)
1/T (K) x 10^4
BF-17
TM-549
93-19A
BF-38B
TM-445
89-22 rim
SP-9B1
89-9 core
89-9 rim
89-22 core
BF-78
ln (ppm Y in garnet) = 16031 ± 862 - 13.25 ± 1.12
T (K)
R² = 0.97
(b)

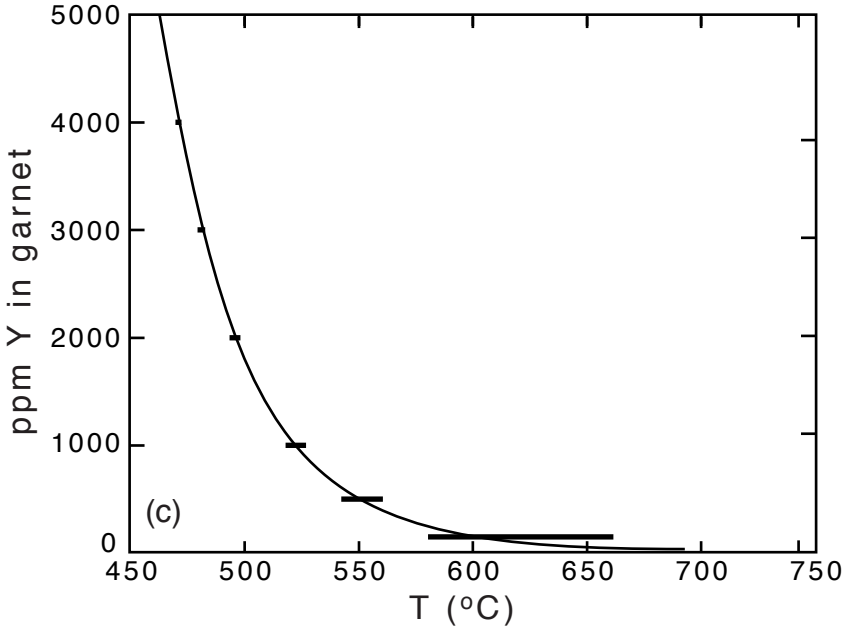
ppm Y in garnet
T (°C)
(c)

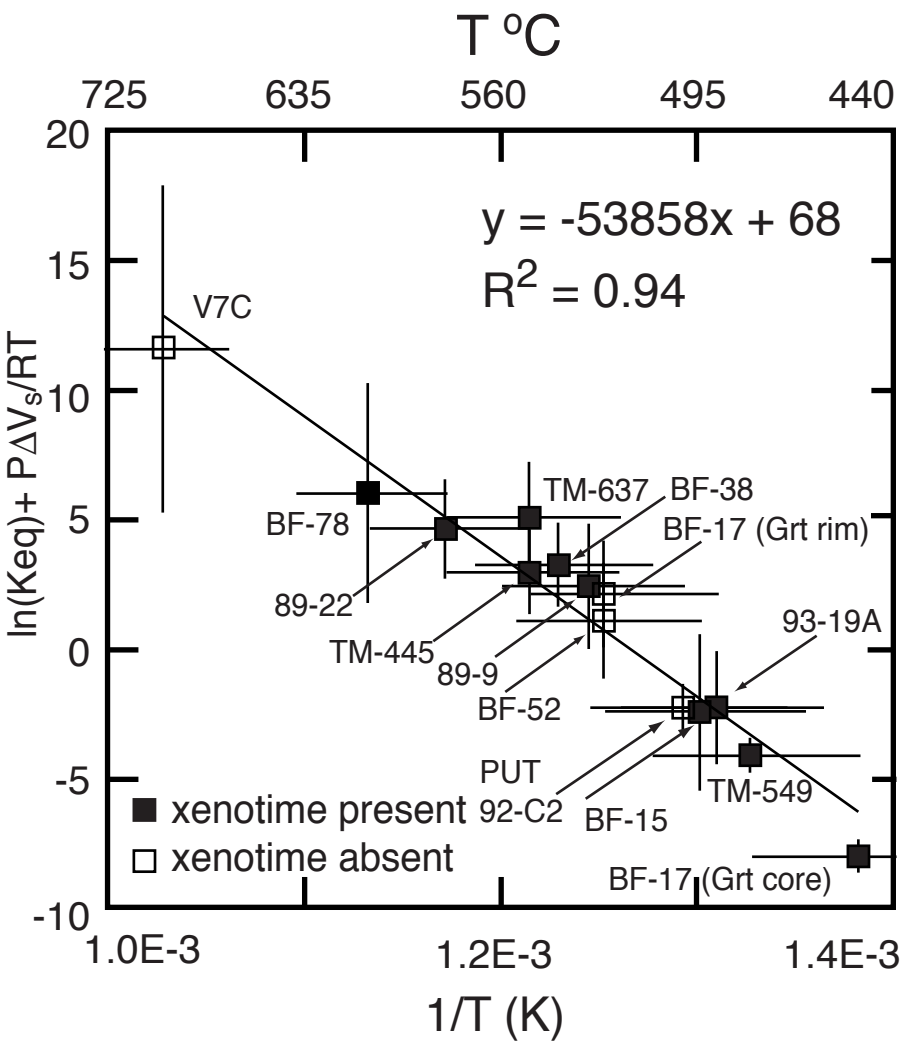
T °C
725
635
560
495
440
20
15
10
5
0
-5
-10
ln(Keq)+ PΔVs/RT
y = -53858x + 68
R2 = 0.94
V7C
BF-78
TM-637
BF-38
BF-17 (Grt rim)
89-22
TM-445
89-9
93-19A
BF-52
PUT
92-C2
BF-15
TM-549
BF-17 (Grt core)
xenotime present
xenotime absent
1.0E-3
1.2E-3
1.4E-3
1/T (K)

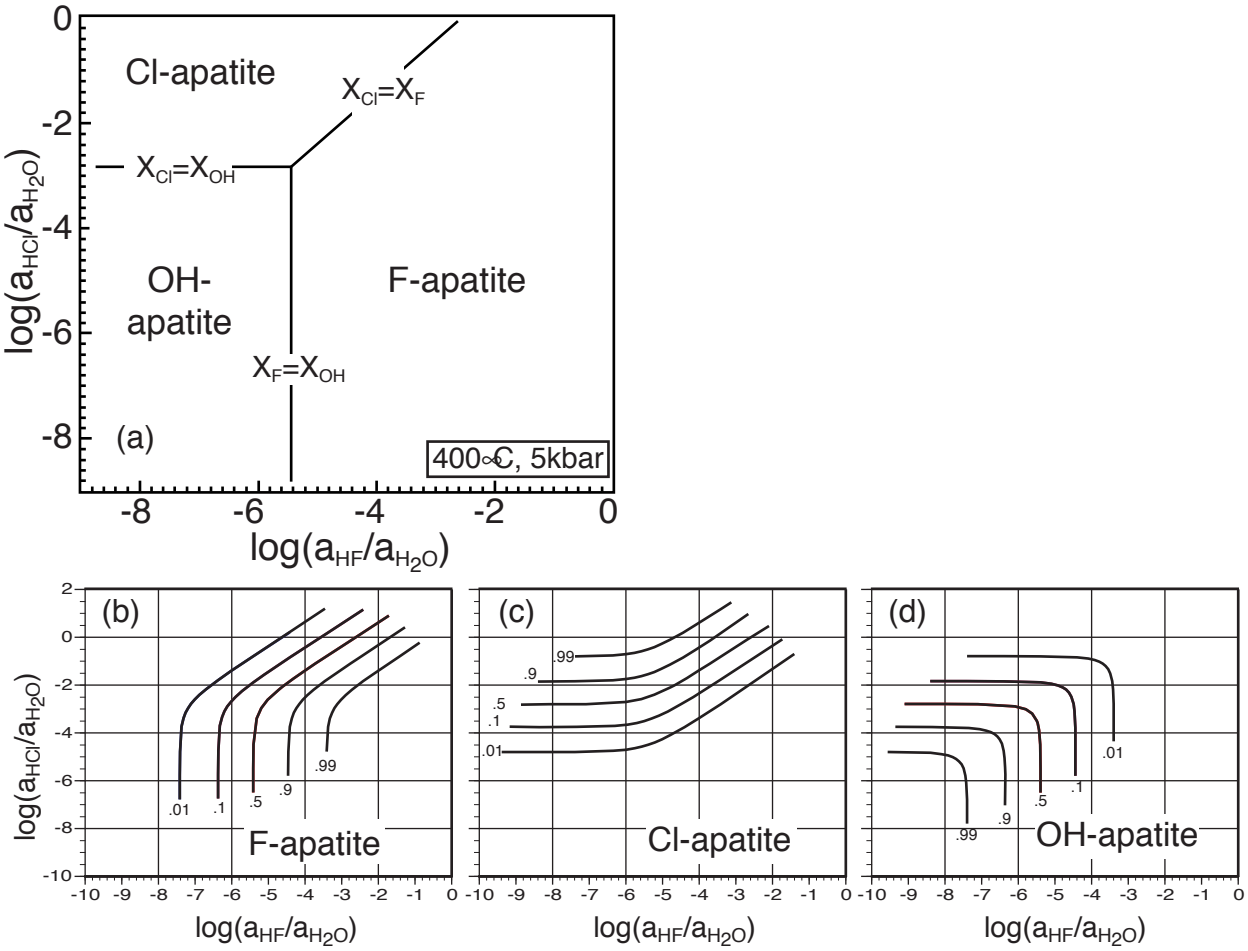
Cl-apatite
$X_{Cl}=X_F$
$X_{Cl}=X_{OH}$
OH-apatite
F-apatite
$X_F=X_{OH}$
(a)
400∞C, 5kbar
$\log(a_{HCl}/a_{H_2O})$
$\log(a_{HF}/a_{H_2O})$
(b)
F-apatite
.01
.1
.5
.9
.99
(c)
Cl-apatite
.99
.9
.5
.1
.01
(d)
OH-apatite
.01
.1
.5
.9
.99